



UNIONE EUROPEA
Fondo Sociale Europeo



Università
degli Studi
della Campania
Luigi Vanvitelli

PhD School in Life Sciences

PhD Course in Translational Medicine

34° cycle

PhD Thesis

Scientific Disciplinary Sector - MED/04

RIPK1-Targeting in cancer: modulation of programmed cell death for cancer treatment



Università
degli Studi
della Campania
Luigi Vanvitelli

**DOTTORATO DI RICERCA IN MEDICINA
TRASLAZIONALE**

Coordinatore: *Prof. Katherine Esposito*

Candidate

Laura Della Torre

Matr. D131000119

Laura Della Torre

Coordinator

Prof. Katherine Esposito

Supervisor

Prof. Lucia Altucci

Academic Year

2021/2022

INDICE

1. SOMMARIO	1
2. ABSTRACT	2
3. INTRODUCTION	3
3.1 EPIDRUGS FOR CANCER CELL DEATH REGULATION	3
3.2 CELL DEATH.....	4
3.3 RIPK1	6
3.4 RIPK1 IN CANCER	9
3.5 RIPK1 IN LEUKEMIA.....	11
3.6 INHIBITORS TARGETING RIPK1 AS A THERAPEUTIC STRATEGY	12
4. AIM OF THE STUDY	15
5. RESULTS	16
5.1 RIPK1 protein expression in cancer cell lines	16
5.2 MC2494 displays context-specific regulation in cancer cell.....	16
5.3 MC2494 impacts on cancer cell migration.....	22
5.4 Study of cell death in U937 cell line	23
5.6 MC2494 regulates mitochondrial function in U937 cell line.....	26
5.5 Several biological processes enriched after MC2494 treatment	29
5.7 MC2494 regulates different biological aspects over time.....	33
5.8 MC2494 modulates RIPK1.....	35
6. DISCUSSION.....	39
7. CONCLUSION.....	41
8. MATERIAL AND METHODS	42
8.1 Cell Line and Culture Conditions	42
8.2 Ligands	42
8.3 Protein extraction.....	42
8.4 Western blot.....	42
8.5 Antibodies.....	43
8.6 Morphological Analysis.....	43

8.7 Wound-Scratch Assay	43
8.8 Boyden's Chamber Assay	43
8.9 Mitochondria Content	44
8.10 Mitochondria Labeling	44
8.11 Immunofluorescence Microscopy	44
8.12 Cell Cycle and Cell Death Analysis	44
8.13 Living Cell Image Detection	45
8.14 Annexin V Staining	45
8.15 Live & Dead assay	45
8.16 ADP-Glo Kinase assay	45
8.17 CETSA assay	46
8.18 Sample preparation for proteomic analysis	46
8.19 High-Resolution NanoLC-Tandem Mass Spectrometry	46
8.20 Protein identification and quantitation	46
8.21 Bioinformatics Analysis	47
8.22 RNA purification	47
8.23 RT-PCR and quantitative real-time PCR analysis	47
8.24 KAPA RNA HyperPrep Kit with RiboErase (HMR)	48
8.25 RNA-seq analysis	48
REFERENCES	49

1. SOMMARIO

La proliferazione, il differenziamento e la morte cellulare sono eventi fisiologici responsabili del mantenimento dell'omeostasi cellulare. Le cellule hanno sviluppato diversi processi per controllare il loro equilibrio omeostatico; infatti, ogni cellula ha un ciclo di vita ben definito al termine del quale va naturalmente incontro a morte. Un'alterazione nei processi di proliferazione e morte cellulare è la causa dell'interruzione dell'equilibrio omeostatico ed è nodo principale di molte malattie, tra cui il cancro. Caratteristica rilevante di una cellula tumorale è sfuggire alla morte cellulare programmata (PCD), andando incontro ad una sregolata proliferazione cellulare e conseguente trasformazione maligna. Recentemente il concetto di morte cellulare si è abbastanza esteso ed il Comitato per la Nomenclatura sulla Morte Cellulare (NCCD) ha formulato linee guida per la definizione e l'interpretazione della morte cellulare dal punto di vista morfologico, biochimico e funzionale. In questo scenario particolarmente notevole si è rivelato essere il ruolo della proteina chinasi RIPK1, la quale interpreta i segnali extracellulari attivando differenti pathway di segnalazione responsabili della sopravvivenza cellulare o della morte cellulare e, sebbene la sua funzione sia ampiamente discussa in patologie infiammatorie, il suo ruolo nel cancro resta ancora da investigare. Il progetto di ricerca proposto ha lo scopo di investigare i meccanismi molecolari che sono alla base di patologie ad elevato impatto sociale come il cancro mediante una migliore caratterizzazione della PCD e di uno dei suoi principali effettori come RIPK1. In questo lavoro sperimentale abbiamo valutato gli effetti biologici di un pan-inibitore delle sirtuine recentemente identificato e caratterizzato, MC2494, per la sua capacità di indurre l'apoptosi *in vivo*, *ex vitro* ed *in vitro* in diversi sistemi tumorali [1]. I nostri risultati hanno dimostrato che l'*epidrug*, nella linea cellulare di leucemia mieloide umana U937, ha la capacità di regolare la morte cellulare mediante la modulazione della funzione di RIPK1. Sebbene questi studi preliminari necessitino un approfondimento, l'MC2494 assume un ruolo chiave nella regolazione della tumorigenesi e nei programmi di PCD mediata da RIPK1, rendendola un evento farmacologicamente controllabile nella terapia del cancro. Questo progetto, inoltre, permetterà lo sviluppo di nuove molecole a scopo diagnostico-terapeutico al fine di capire, per future applicazioni cliniche, come modulare il complesso RIPK1 nella morte cellulare in cancro.

2. ABSTRACT

Proliferation, differentiation, and cell death are physiological events responsible for the maintenance of cellular homeostasis. Principal characteristic of tumor cell is to escape programmed cell death (PCDs) processes, going to a consequent malignant transformation. Disruption of homeostasis, particularly through alterations in the regulation of cell proliferation and cell death may be mediated by Receptor-interacting serine/threonine-protein kinase 1 (RIPK1). RIPK1 takes part in several signaling pathways involved in kinase dependent and independent tasks resulting in cell survival or cell death to regulate homeostasis. Furthermore, although its function is widely discussed in inflammatory conditions, little is known about the biological relevance of RIPK1 in cancer. A major goal is to understand “how” RIPK1 triggers different cellular pathways that leads cells to make a critical decision either to survive or die. The proposed research project aims to highlight the molecular mechanisms underlying diseases with a high social impact such as cancer through a better characterization of PCD and its main effector RIPK1. Furthermore, the project will allow the development of new molecules for diagnostic-therapeutic purposes to understand, for future clinical applications, how to modulate the RIPK1-mediated complex and cell death in the tumorigenesis process.

3. INTRODUCTION

3.1 EPIDRUGS FOR CANCER CELL DEATH REGULATION

Growing evidence suggests that aberrant epigenetic regulation of gene function is strongly related to the genesis of cancer. The epigenetic mutations (*epimutations*) in tumor cells induce changes in the phenotype and in the stability of the genome, then they have been considered driver mutations in the tumours and, together with genetic lesions, they promote carcinogenesis [2]. However, unlike genetic mutations, epigenetic alterations are potentially reversible and have great plasticity, as the epigenome can be reprogrammed. The possibility of reprogramming the epigenome represents a new and promising therapeutic strategy [3]. It is becoming increasingly clear that cancer is not only a genetic but also an epigenetic disease therefore epigenetic therapy represents today one of the most interesting perspectives to correct pharmacologically some of the anomalies involved in the onset of neoplastic diseases [3]. The design of therapeutic strategies involving epigenetic drugs (*epidrugs*) is a growing field of drug discovery, which focuses on the cancer epigenome to develop pharmacological compounds which could restore a normal epigenetic landscape in different pathological conditions [3].

Epidrugs are small molecules of synthetic or natural derivation that target specific epigenetic modifications. These molecules, in addition to regulate the functional state of chromatin, are able of both reactivating the expression of silenced tumor suppressors and DNA repair genes, and restoring the correct functioning of specific cellular pathways such as cell death, inhibited in many pathologies, including cancer [3]. The use of epidrugs represents a promising perspective in the medical field of research which lead to the approval by the *American Food and Drug Administration* of drugs with epigenetic activity, able to restore the correct functioning of some genes with a certain relevance for cellular activity [4]. Thanks to their therapeutic properties and low toxicity, they can be more active in neoplastic systems and not act or act less in normal cell systems. Regarding their selectivity, the most confirmed hypothesis concerns the ability of these compounds to reactivate cellular signal transduction pathways, silenced only in tumor cells [4]. The use of epidrugs in single- or multi-drug therapy, or immunotherapy has shown an improvement in the efficacy of treatments, reactivating silenced cellular pathways such as those of regulated cell death, resulting in a greater degree of tumor remission, reduction of chemoresistance, increase in life expectancy and reduction of side effects.

Sirtuins are currently considered as attractive molecules for their potential as a new category of anticancer agents [5]. Recent studies proposed that triggering of cell death by sirtuin inhibitors, besides relying on re-expression of epigenetically inactivated genes, may arise from hyperacetylation of heterochromatic regions (e.g., centromeres), which leads to aberrant mitoses and subsequent activation of PCD. Irrespective of what is the triggering mechanism, the induction of PCD still represents a common effect in neoplastic cells treated with epigenetic drugs [5].

3.2 CELL DEATH

Each cell has a well-defined life cycle at the end of which it dies naturally. Cell death has a pivotal role for the life of an organism, but resistance to this process represent one of the most important hallmarks in cancer. Conceptually, cell death is defined as the permanent degeneration of vital cellular functions. Technically the precise boundary between a reversible alteration of homeostasis and the irreversible loss of cellular activities resulting in cell death seems difficult to identify. Cell death can be classified into two broad categories that are mutually exclusive: accidental and regulated. Accidental cell death (ACD) is a catastrophic and extreme event with consequent disruption of cellular structure since it is completely unprogrammed [6]. In contrast, regulated cell death (RCD) is a controlled process, depending on activation of signaling cascades and hence can be genetically and pharmacologically controlled. When RCD occurs in strictly physiological scenarios in the context of tissue homeostasis and immune responses it is referred to programmed cell death (PCD) [7] (Figure 1).

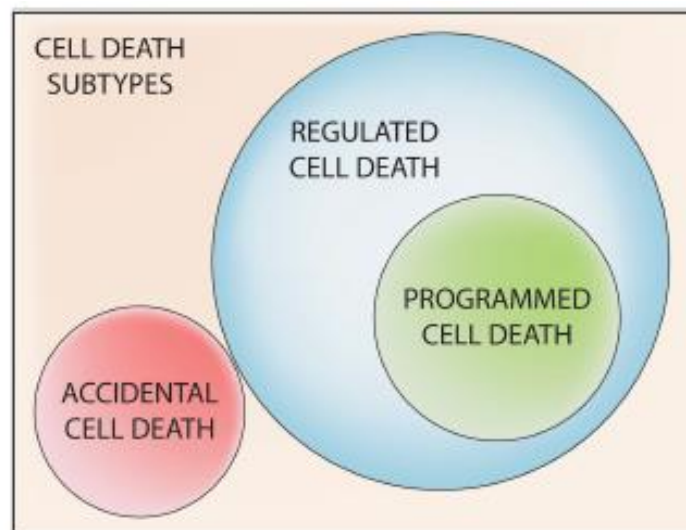


Figure 1. Types of cell death. [6].

Apoptosis and necrosis were the first and so the best known two modalities of cell death discovered. Historically, apoptosis has been associated with non-immunogenic, regulated, and programmed form of death, while necrosis has been defined as accidental and uncontrolled [8]. Apoptosis is a defence mechanism that occurs physiologically as a result of extracellular or intracellular microenvironment perturbations and is mediated by a specific class of cysteine protease named caspases [9]. After extracellular or intracellular apoptotic stimuli, caspases activate the molecular pathways needed to eliminate damaged cells [7]. Conversely, necrosis is the result of accidental events induced by different stimuli such as osmotic variations, arrest of the supply of nutrients, protein denaturation and it is characterized by a robust inflammatory and immunogenic response [6,8,9]. Since 2005 the Nomenclature Committee on Cell Death (NCCD) has

formulated a series of recommendations to help scientists and researchers to discriminate essential and accessory aspects of cell death by overcoming the limitations of morphological criteria alone. The updated classification of major cell death subroutines divides RCDs into 12 classes whose molecular and biological mechanisms need to be better clarified: intrinsic apoptosis, extrinsic apoptosis, MPT-driven necrosis, necroptosis, ferroptosis, pyroptosis, parthanatos, entotic cell death, NETotic cell death, lysosome-dependent cell death, autophagy-dependent cell death, and immunogenic cell death (Figure 2) [7].

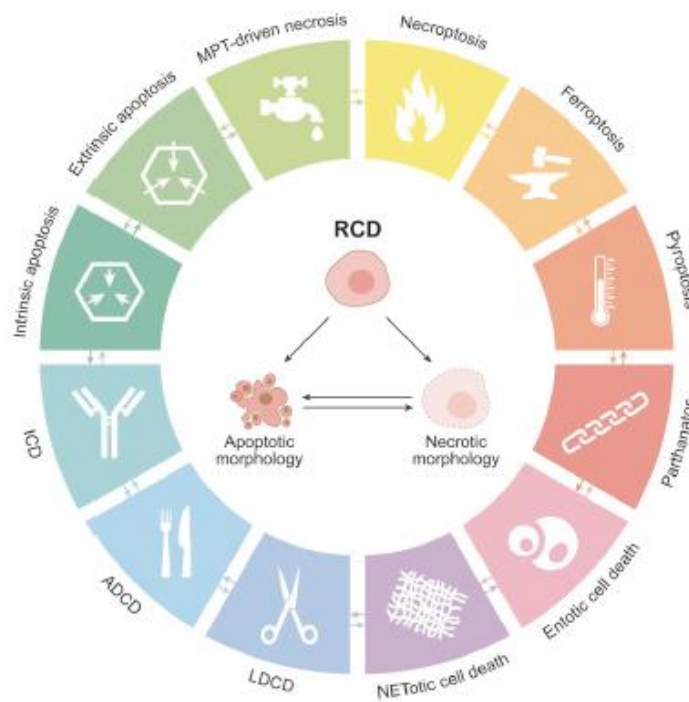


Figure 2. Major cell death subroutines [7].

The different RCDs exhibit a considerable degree of interconnectivity although each one is characterized by a specific signal transduction cascade and morphological, biochemical, and immunogenic features as biomarkers. Deregulation of cell death in cancer can lead to drug resistance and consequently to therapeutic failure, so it is necessary to strongly strengthen the idea that PCD targeting in tumorigenesis can represent a strategic tool in oncology [10]. The loss of the ability to regulate cell death allows cells to survive even in unfavourable conditions, giving longer times for the accumulation of mutations that can increase invasive capacity during cancer progression, stimulate angiogenesis, deregulate cell proliferation, and interfere with differentiation.

Among the 12 RCDs, necroptosis is the first form of programmed necrosis described with a prominent role in multiple physiological and pathological conditions [8]. Necroptosis occurs in several biological processes, including inflammation, immune response, embryonic development, and metabolic alterations. Numerous

evidences also suggest the involvement of this cell death in the pathogenesis of diseases including organ injury, neurodegenerative diseases and viral infections [11,12]. Furthermore, necroptosis seems to control the homeostasis of T cells by eliminating the abnormal and excess ones in caspase-8 deficient T cells [13]. In addition to these physio-pathological functions, it shows a contradictory role in cancer that needs to be better investigated since several studies suggest its involvement as a cancer suppressor, while others as cancer promoter [14,15]. Necroptosis in cancer can be described as a 'double-edged sword' because its induction supports the death of abnormal cells leading to a good prognosis; on the other hand, in the same pathological conditions, necroptosis could determine the activation of alternative pathways and evoke inflammation, complicating cell fate and the outcome of the pathologies leading to cancer metastasis [15,16]. The necroptotic process is induced by different extracellular or intracellular stimuli and detected by specific death receptors, pathogen recognition receptors and Z-DNA binding protein 1 (ZBP1 also called DAI) [7,17]. Morphologically, it is like to necrosis and is characterized by an early loss of membrane integrity, an increase in cell volume and organ swelling [18]. At biochemical level, the mitochondrial fission, the production of reactive oxygen species (ROS), the depletion of ATP and the entry of ions such as sodium and calcium are observed [19]. At molecular level, necroptosis is characterized by the inactivation of caspases and is controlled by the kinase activity of two members of the Receptor-Interacting serine/threonine-Protein (RIP) kinases family, in fact the necroptotic core is constituted by RIPK1, RIPK3 and mixed lineage kinase domain such as (MLKL) [7]. The well-studied executor, RIPK1, can modulate key cellular events through the interaction with several proteins, acting as strategic crossroads of several molecular pathways. It may mediate the disruption of homeostasis through alterations in the regulation of cell proliferation and cell death. Since recent evidence has also suggested that RIP1 kinase activity may participate in the tumorigenesis process and its expression is deregulated in certain types of human cancer tissues, it seems to be a good candidate for future investigation [15,20].

3.3 RIPK1

RIPK1 is the first member of a 7-member family to be identified, who share a homologous kinase domain and participate in specific biological processes based on their functional domains. It consists of a kinase domain (KD) at the C-terminus and a death domain (DD) at the N-terminus. Furthermore, RIPK1 hosts the RIP homotypic interaction motif (RHIM) in the intermediate region (Figure 3) [21]. RIPK1 has been defined as an "enigmatic signal adaptor" due to its pleiotropic functions in several signaling pathways involved in kinase dependent and independent tasks resulting in cell survival or cell death to regulate homeostasis leading to inflammation and apoptotic or necroptotic cell death [22].

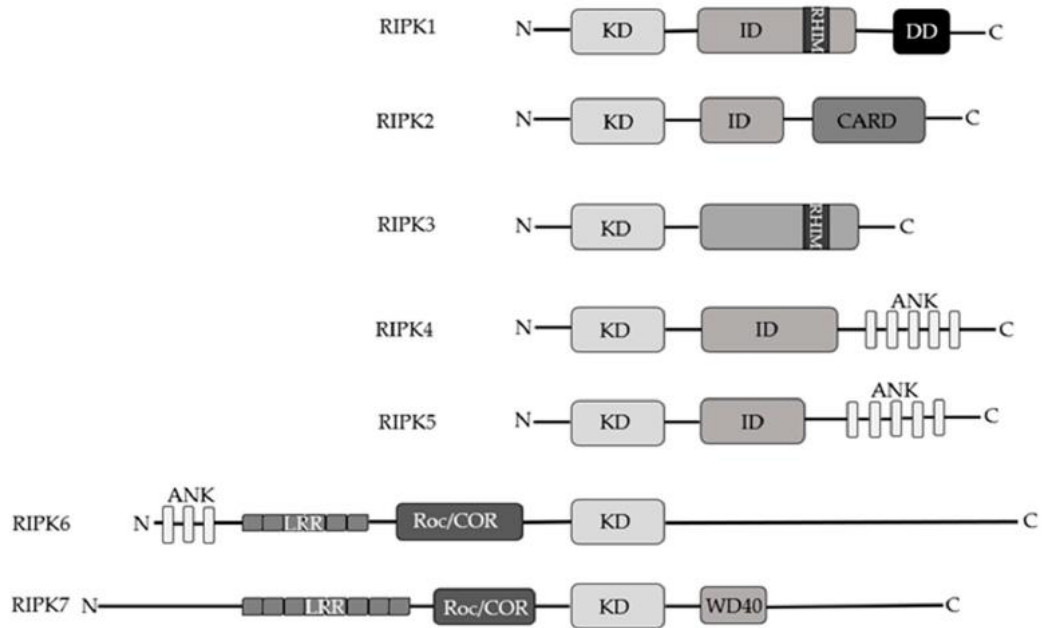


Figure 3. Schematic representation of RIP kinases family's members [21].

RIPK1 gene maps to chromosome 6p25.2 based on an alignment of the RIPK1 sequence (GenBank AB208926) with the genomic sequence (GRCh37). The gene is constitutively transcribed in many tissues with a different degree of expression and it is known to participate in chromosomal stability [23]. Several transcripts have been identified but only two are the sequences encoding the RIPK1 protein. The best characterized isoform has a length of 671 amino acids with a molecular weight of 75.9 KDa and, recently a new variant of alternative splicing has been discovered which differs from the first in the lack of 46 amino acids in the kinase domain with a molecular weight of 70.7 KDa [uniprot.org].

RIPK1 is present in protein complexes that mediate signal transduction from cell surface receptors. A range of stimuli, such as ligands for tumor necrosis factor receptor (TNFR), interferon-alpha receptor (IFN α R), and Toll-like receptor (TLR) families, as well as viral infection and genotoxic stressors have been associated with RIPK1 activation characterized by the formation of a specific molecular complex [17,24]. Upon TNF stimulation, RIPK1 is recruited into TNFR1 through the homotypic membrane-associated DD interaction. In the pro-survival complex, named complex I, RIPK1 is associated with Tumor necrosis factor receptor type 1-associated death domain protein (TRADD), TNF receptor-associated factor (TRAF1/2/5), cellular inhibitor of apoptosis protein-1 and -2 (cIAP1/2), linear ubiquitin chain assembly complex (LUBAC), NF-kappa-B essential modulator (NEMO), and deubiquitinating enzymes. RIPK1 is rapidly polyubiquitinated on residues K63-linked and M1-linked ubiquitin chains mediated by cIAP1/2 and LUBAC, which in turn recruit MAP3K7-binding protein 2, 3 (TAB2/3) and NEMO respectively. NEMO recruitment in the complex I is mostly, but not exclusively, M1-ubiquitin dependent, and mediates serine/threonine-protein kinase TBK1 and inhibitor of

nuclear factor kappa-B kinase subunit epsilon (IKK ϵ) activation whose recruitment is also allowed by LUBAC activity [25]. TBK1 and IKK ϵ phosphorylate RIPK1 on multiple residues preventing RIPK1-dependent cell death [25,26]. Additionally, K63 ubiquitination on RIPK1 mediates TAB2/3 recruitment facilitating mitogen-activated protein kinase kinase kinase 7 (TAK1) activation, that phosphorylates IKK α/β and RIPK1 [25]. The formation of the IKKs complex and the phosphorylation of RIPK1 on serine 25 residue by IKK α/β promote the activation of Nuclear factor kappaB (NF- κ B) and mitogen-activated protein kinase (MAPK) signaling pathways suppressing RIPK1-mediated necroptosis and apoptosis [27,28]. Following cIAPs degradation by small pharmacological compounds, deubiquitinase enzymes negatively affect the ubiquitination of RIPK1 by promoting the formation of a new molecular complex, complex II, also referred as ripoptosome [29]. In ripoptosome RIPK1 associates with TRADD, FAS-associated death domain protein (FADD), and pro-caspase 8 forming Complex IIa where activated caspase-8 cleaves RIPK1 and RIPK3 to promote RIPK1-independent apoptosis (RIA) [30]. After Smac mimetic molecule activity, which promotes a reduction in RIPK1 ubiquitination and consequent activation of Caspase-8, activated RIPK1 can interact with FADD and caspase-8 to mediate RIPK1-dependent apoptosis (RDA) in the complex IIb [31]. If caspase-8 is inhibited or absent and RIPK3 and MLKL expression levels are high in the cells, RIPK1 can start a series of auto and trans-phosphorylation events with RIPK3 which lead to MLKL activation to form the downstream necrosome complex IIc beginning the necroptosis process (Figure 4) [32]. In addition to RIPK1, RIPK3 can also be activated by interaction with other RHIM-containing proteins such as the toll-like receptor adapter protein TRIF and the cytosolic ZBP1. Paradoxically, RIPK1 has been found to inhibit TRIF-RIPK3 and ZBP1-RIPK3 necrosomes in an RHIM-dependent and kinase-independent manner under certain conditions [33]. Therefore, the scaffold and kinase functions of RIPK1 promote cell survival and death respectively, making of RIPK1 a target for pharmaceutical attempts. Furthermore, the role of RIPK1 strongly depends on post-translational modifications, mainly phosphorylation and ubiquitination, which can lead to different functions of RIPK1 in different signaling pathways. Although abundant advances are evident in describing the molecular mechanisms involving RIPK1 in the field, the crosstalk complex in its roles in cell death *vs* survival makes it difficult to determine the precise events that regulate RIPK1 signaling [34,35].

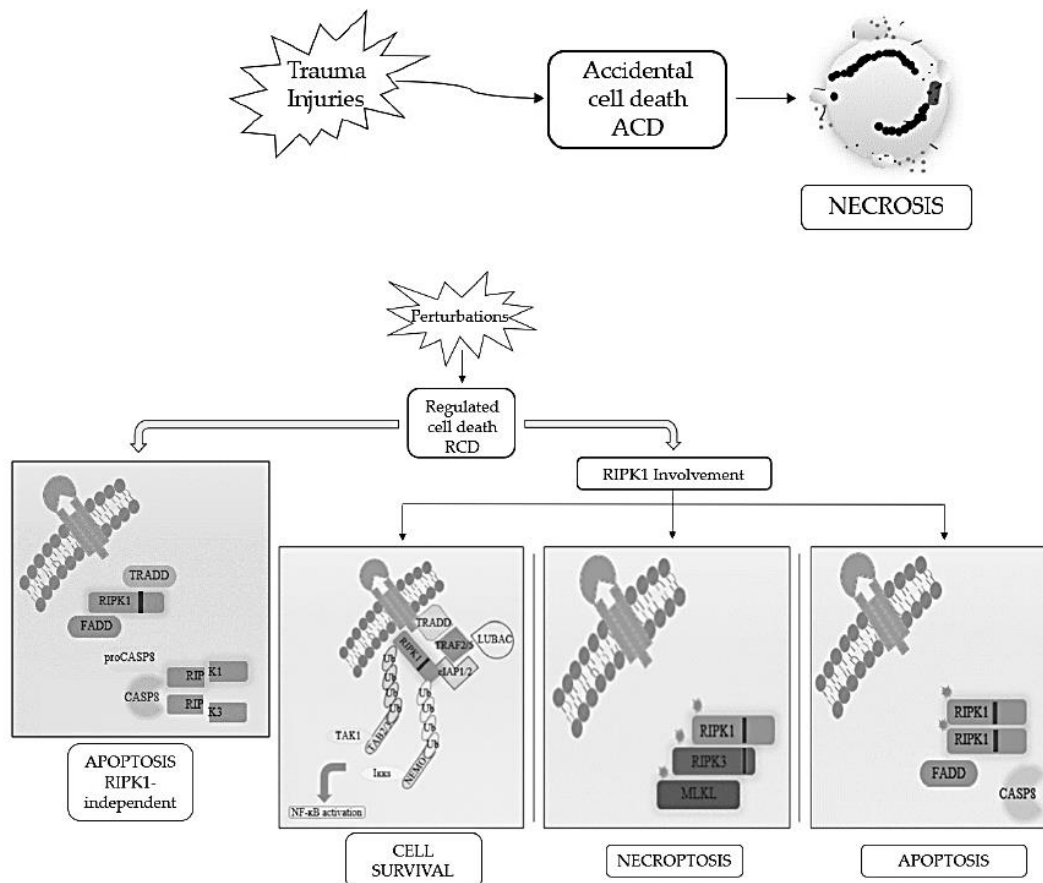


Figure 4. Schematic representation of the best-known cell death modalities with different molecular features [36].

3.4 RIPK1 IN CANCER

RIPK1 activity has been implicated in a wide range of pathological processes such as ischemic damage, inflammatory diseases, axonal degeneration, and auto inflammatory and autoimmune diseases. Recent evidence also suggests that the activity of this kinase may participate in tumorigenesis [32]. RIPK1 exhibits from weak to moderate cytoplasmic localization in most cancerous tissues and its altered expression levels impact in cancer [37]. RIPK1 is frequently upregulated or downregulated in cancer depending on the genetic and cellular context and the functional mutations that can compromise the death of cancer cells and influence the prognosis due to changes in interactions between RIPK1 and other proteins [20]. Depending on the specific cancer types, RIPK1 can be oncogenic or tumour suppressor. The double roles most likely reflect the functions of this kinase in cell survival, cell death and inflammation. Over the years, interest in the correlation between gene mutations associated with RIPK1 and cancer has grown. Furthermore, as reported by the COSMIC database about the somatic mutations in cancer, RIPK1 gene is not significantly mutated in a specific tissue, rather, the identified mutations are: about 36% missense substitutions, 10% synonymous substitutions, 5% nonsense substitutions, 0.4% frameshift insertions, 0.2% frameshift deletions and 9% of mutations without

detailed information available [38]. *Ripk1* belongs to those genes with a part probably implicated in cancer and the ICGC database reported genomic and proteomic mutations in cancer distribution (<https://dcc.icgc.org/>). Many genetic alterations, mainly amplification and genomic mutations, have been described for RIPK1 in human cancer [37]. Furthermore, epigenetic events such as the methylation status in the *RIPK1* promoter can influence its regulation in cancer [36]. RIPK1 is commonly downregulated in breast cancer, colorectal cancer (CRC), head and neck squamous cell carcinoma (HNSCC) and liver cancer [37,39–41]. Low expression of RIPK1 in patients with hepatocellular carcinoma undergoing liver resection or transplantation predicted poor prognosis and low RIPK1 expression in triple negative breast cancer was associated with worse clinical outcomes [40,41]. In glioblastoma, lung cancer, melanoma, pancreatic ductal adenocarcinoma (PDA), gastric cancer and gallbladder cancer its expression has been found to be upregulated, affecting cancer prognosis negatively [42–47]. High RIPK1 protein expression in glioblastoma grade IV but not in lower grade glioma (I–III), has been associated with reduced overall survival supporting its oncogenic role [42]. Similarly, RIPK1 expression was found to be upregulated in melanoma tumor through a positive feedback loop of NF- κ B-BIRC2/BIRC3-RIPK1 powered by autocrine tumor necrosis factor suggesting that RIPK1 promotes cell survival in melanomas [46]. RIPK1 also revealed to be more likely involved in the metastatic process of monosomy 3 in uveal melanomas [48]. A recent study suggests the oncogenic function of RIPK1 in the lung epithelial cells that have acquired genetic mutations and epigenetic modifications caused by carcinogens [43]. Recently the high level of *RIPK1* expression in urothelial cancer has been associated with a favourable prognosis with significantly higher overall survival for patients [proteintlas.org] (Table 1). Finally, in ovarian cancer, RIPK1 appears to play a dual role, in which kinase depletion resulted in reduced proliferation but also reduced sensitivity to cisplatin treatment stressing, once again, the dual role of RIPK1 in both cell survival and cell death [49]. Then, it would be interesting to determine in some cancers whether RIPK1 is initially upregulated to promote cell proliferation and ultimately downregulated during cancer progresses to suppress its ability to induce cell death.

	Alteration and cancer types	References
RIPK1	<u>Downregulation:</u> Breast, CRC, HNSCC, Liver	[37,39–41]
	<u>Upregulation:</u> Gallbladder, Gastric, Glioblastoma, Lung, Melanoma, PDA, Urothelial	[42–47]

Table 1. Deregulated expression of RIPK1 in some tumours.

Additionally, RIPK1 is part of those fusion genes that play a key role in tumorigenesis in fact it belongs to the genes involved in translocations found in adenocarcinoma of the breast, prostate, and ovary (Table 2). *RIPK1* has been found also in Astrocytoma, Grade III-IV/Glioblastoma in which translocation t(6;6) (p25: p25) occurs.

Morphology- Topography	Genes	Abnormality	References
Breast Adenocarcinoma	RIPK1/BCKDHB	t(6;6) (p25;q14)	[50]
Breast Adenocarcinoma	RIPK1/NQO2	t(6;6) (p25;p25)	[51]
Prostate Adenocarcinoma	FARS2/RIPK1	t(6;6) (p25;p25)	[50] [52]
Brain Astrocytoma, grade III- IV/Glioblastoma	RIPK1/SERPINB9	t(6;6) (p25;p25)	[53]
Ovary Adenocarcinoma	RIPK1/TTC27	t(2;6) (p22;p25)	[50]

Table 2. RIPK1 fusion gene involved in tumorigenesis [36].

Currently, the role of RIPK1 in leukemia is still much discussed and therefore unclear. Its heterogeneity expression levels in leukemia patient samples and its relevance because of the diverse functions suggest to define as soon as possible its role in the haematological malignancies [54]. Considering the several types of leukemia it is quite difficult to define properly the biological function of RIPK1 in order to promote leukemia cell death.

3.5 RIPK1 IN LEUKEMIA

In hematopoietic tissues RIPK1 seems to maintain the homeostasis by preventing TNF-induced apoptosis and IFN- γ or TLR signaling-stimulated necroptosis [55]. It is important to underline that necroptosis in leukemia may be prevented by the potent oncogene MYC, which after necroptotic stimuli, inhibits the spontaneous interaction of RIPK1 with the other necrosome components [56]. Moreover, acute myelomonocytic leukemia and acute monoblastic leukemia (AML) (M4 and M5 subtypes in acute myeloid leukemia, respectively) show

basal level activation of necrosome components whose activation is required for maintaining the undifferentiated state of such malignant cells [55]. This study suggested that RIPK1 inactivation may be an effective treatment for AML patients when combined with specific chimeric antigen receptor T cells (that express high levels of IFN- γ) or other differentiation inducers to repress leukemogenic capacity of AML cells [55]. In addition, RIPK1 is among the protein substrate of caspase-8 for physiological monocyte differentiation triggered by colony-stimulating factor 1 receptor (CSF1R) that is clearly altered in chronic myelomonocytic leukemia (CMML) [57]. Furthermore, elevated *RIPK1* expression using CD34+ bone marrow (BM) cells from patients with CMML has been defined as an independent adverse prognostic factor and has been associated with significant overexpression of genes involved in TNF- α and NF- κ B signaling, RIG-I-like receptor (RLR) signaling genes and IFN- γ pathway supporting the association of *RIPK1* with innate immunity and pro-inflammatory signaling in myelodysplastic syndrome (MDS) BM CD34+ cells [58]. Moreover, the increased expression of RIPK1 and phospho-MLKL observed in MDS patients with multilineage dysplasia compared with those with excess blasts suggests that necroptosis may be activated during the early stage of the disease while during the progression, additional genomic and epigenomic abnormalities may lead to escape cell death thus facilitating progress disease [58]. In this scenario, increased RIPK1 expression levels at the time of diagnosis has been defined as a mediator of inflammation and a predictor of worse overall survival [58]. Another study revealed that in CD34+ blasts from AML patients the expression of RIPK1 allows malignant cells to suppress various functions, including necroptosis, apoptosis and modulation of the NF- κ B pathway [59]. The use of a dedicated DNA chip containing 16,561 single nucleotide polymorphisms (SNPs) covering 1,916 candidate genes to analyse CML patients and healthy control subjects revealed that individuals with haplotypes containing three rare alleles for the RIPK1 gene along with other genes have a higher risk of developing chronic myeloid leukemia [60]. Additionally, both SNP and gene-based analyses showed the risk of childhood leukemia associated with some genes included RIPK1 [61]. In adult T-cell leukemia/lymphoma (ATLL) RIPK1 is defined as a sensitive key mediator of death signaling because its K63-ubiquitination status controlled by the increased level of the deubiquitinase CYLD determines cell fate by creating either a pro-survival signal (ubiquitinated RIPK1) or a death signal (deubiquitinated RIPK1) [62]. Importantly, in childhood acute lymphoblastic leukemia (ALL) cells RIPK1 is a critical regulator for chemotherapy-induced apoptosis in a RIPK1-dependent manner considering that the synergism of inhibitors of apoptosis and various anticancer drugs mediates the formation of a RIPK1/FADD/caspase-8 complex via an autocrine/paracrine loop of TNF α [63].

3.6 INHIBITORS TARGETING RIPK1 AS A THERAPEUTIC STRATEGY

Impairment of cell death pathways and evasion of RCD are hallmarks of tumorigenesis; indeed, they contribute to tumour initiation, progression, and treatment resistance. Resistance to chemotherapy is currently a major problem in cancer treatment, and it is frequently associated with failure of tumor cells to undergo

apoptosis. Therefore, there is an urgent need to develop new therapies to promote cell death in cancers [64]. Overall, modulating RIPK1 may result in powerful anti-cancer effects. In some cases, promoting RIPK1-dependent cell death may be highly beneficial, while in other cases reducing necrosome-dependent inflammation, driving immune suppression by tumor-infiltrating myeloid cells, may be highly beneficial, stressing also in this case the dual functional role of RIPK1. Recently, it has also been displayed that RIPK1 kinase activity inhibition enhance antitumor immunity through modulation of tumor-associated macrophages [65]. Furthermore, while these responses have been, thus far, examined separately, the possibility remains that inhibition of RIPK1 may simultaneously promote both pro- and anti- tumor responses [32]. Then, clarify "how" RIPK1 regulates the outcomes of the different cellular pathways and its involvement in the tumorigenesis, increases and strengthens the already well-discussed concept of "personalized therapy". Starting from Necrostatin-1s (Nec-1s), the first small molecule inhibitor of RIPK1 kinase activity, many drugs development programs have pursued targeting RIPK1 [66]. The protein contains a unique hydrophobic pocket that allosterically regulates the activation of its kinase activity indeed all RIPK1 inhibitors described to date bind to this pocket and stabilize the kinase in an inactive conformation [65]. Until now, few molecules have been identified to target RIPK1, which led to the first RIPK1 kinase inhibitor (GSK2982772) entering clinical trials for the treatment of inflammatory disorders, such as ulcerative colitis, psoriasis, and rheumatoid arthritis. The brain penetrant DNL747 is in human clinical trial phase Ib/IIa for amyotrophic lateral sclerosis (ALS) while GSK3145095 showed encouraging preclinical data for treating pancreatic cancer but now the drug has been ruled out. Unfortunately, clinical trials of RIPK1 inhibitors for the treatment of solid tumours have not succeeded (Figure 5).

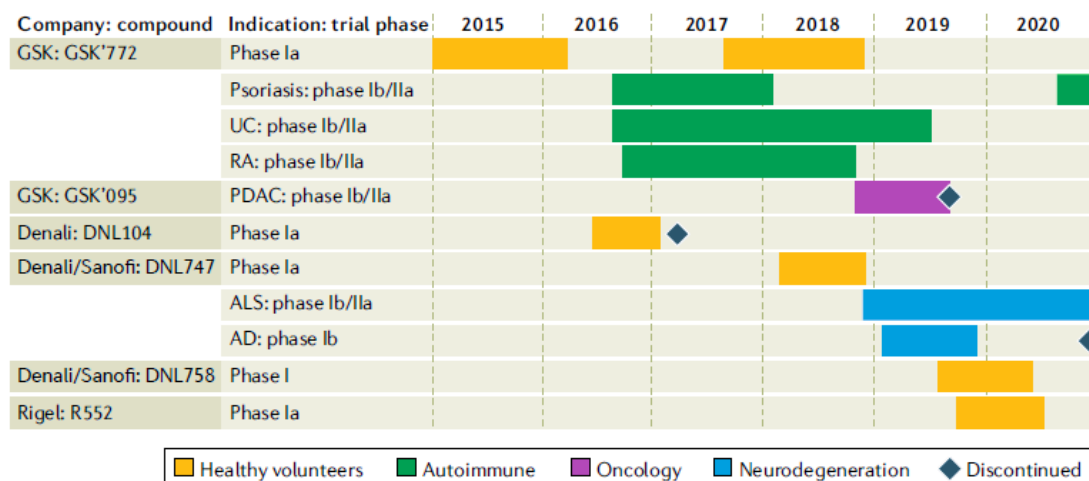


Figure 5. Overview of RIPK1 inhibitor clinical trials [67].

In addition, several approved kinase inhibitors even off-target may lead to sensitization of the RIPK1-mediated pathways (Figure 6) [65]. Development of selective, powerful, and safe molecules inhibitors of RIPK1, biomarkers to reliably measure the clinical efficacy of RIPK1 kinase inhibition remain key challenges facing future clinical development.

Name	Company	Targets	Status	Therapeutic application	RIPK1/3 disease model
Kinase inhibitors that block RIPK1 and/or RIPK3 as off-target kinases					
Sorafenib (Nexavar)	Bayer, Onyx	RAF, PDGFR, VEGFR, FGFR, FLT3, RET, KIT, RIPK1, and RIPK3	FDA approved	Advanced liver cancer; renal cancer; thyroid cancer	TNF-induced SIRS, kidney ischemia/reperfusion injury
Sunitinib (Sutent)	Pfizer	VEGFR, PDGFR, KIT, RET, CSF-1R, FLT3, and RIPK1	FDA approved	Renal cancer and intestinal cancer (gastrointestinal stromal tumors)	NT
Pazopanib (Votrient)	GSK, Novartis	VEGFR, PDGFR, KIT, FGFR, ITK/TSK, SH2B3, and RIPK1	FDA approved	Advanced renal cancer, soft tissue sarcoma, and thyroid cancer	NT
Tozasertib (VX-680)		Pan-Aurora kinase, ABL, FLT3, and RIPK1	Discontinued	Colorectal cancer, CML and ALL	TNF-induced SIRS
Ponatinib (Iclusig)	Ariad, Millennium Pharmaceutical	BCR-ABL, VEGFR, PDGFR, FGFR, EphA2, SRC, KIT, RET, TIE2, FLT3, TAK1, RIPK1, RIPK2, and RIPK3	FDA approved	CML and ALL	TNF-induced SIRS
Dabrafenib (Tafinlar)	GSK, Novartis	BRAF, RAF, SIK1, NEK11, LIMK1, RIPK3	FDA approved	Metastatic melanoma	Acetaminophen-induced liver injury and ischemic brain injury
'Specific' RIPK1 inhibitors					
GSK2982772	GSK	RIPK1	Phase II	Psoriasis, ulcerative colitis, and rheumatoid arthritis	TNF-induced SIRS and ulcerative colitis
GSK3145095	GSK	RIPK1	Phase I/II: terminated	Pancreatic cancer	U
DNL747	Sanofi, Denali Therapeutics	RIPK1	Phase I	Alzheimer's disease, amyotrophic lateral sclerosis, and multiple sclerosis	U

^aAbbreviations: ALL, acute lymphoid leukemia; CML, chronic myeloid leukemia; NT, not tested; SIRS, systemic inflammatory response syndrome; U, unknown (information available from the website of the company, but no structure or publications available yet).

^bData from drugbank.ca and clinicaltrials.gov.

Figure 6. Overview of approved kinase inhibitors that Block RIPK1 and/or RIPK3 as off-target kinase and specific RIPK1 inhibitors that reached clinical trials [65].

Hence, RIPK1 has emerged as a promising target for a spectrum of several pathologies but further studies are needed to better delineate how RIPK1 affects the treatment response of different types of cancer since its activation may not always be a beneficial anticancer strategy as this kinase has also been shown to promote tumorigenesis in some settings [32].

4. AIM OF THE STUDY

How organisms regulate the correct balance between the production of "new" cells and the elimination of the "old" ones, remains an important biology issue under investigation, considering that many pathologies arise through disruption of homeostasis. Principal characteristic of tumour cells is to escape from PCD, going to an unregulated cell proliferation and consequent malignant transformation. Some types of tumours, with a common feature of low survival rate already one year after diagnosis, are grouped as "poor prognosis cancers". Among them, acute myeloid leukaemia (AML) has a 5-year survival of 40%; thus, to develop of novel more selective and specific treatments is currently an 'unmet' need. Although the involvement of RIP1 in regulating inflammatory processes is well studied, little is known about its function in tumorigenesis. Recently, was identified a new protein complex in which RIP1 interacts with the sirtuins (SIRT1 and SIRT2) and with the acetyltransferases (HAT1 and HAT4), suggesting a role for RIP1 (de)acetylation in modulating PCD.

The research project aims to highlight the molecular mechanisms underlying diseases with a high social impact such as cancer, through a better characterization of necroptosis, one programmed cell death process and one of its main effectors such as RIPK1.

The investigation of the interconnection between apoptosis and necroptosis (or other PCD pathways) is currently poorly characterized and both modulation and restoration of the PCDs equilibrium might represent a therapeutic strategy in cancer therapy, and in particular in AML.

To this aim we will investigate the biological activity of the novel characterized pan-sirtuin inhibitor, MC2494, highlighting its anti-cancer role, defining the effects of the compound on cell cycle progression, cell death regulation and cell migration.

A deep characterization of cell death mechanisms will be studied in order to better understand "how" RIPK1 is able to that modulate the equilibrium between apoptosis, necroptosis and survival identifying it as a death player altered in leukemia.

5. RESULTS

5.1 RIPK1 protein expression in cancer cell lines

To evaluate the biological function of RIPK1 in cancer tumorigenesis, its protein expression was assessed in different cancer cell lines from solid and haematological tumours through Western blot analysis from whole cellular extract (Figure 7). The protein was ubiquitously detected in all cancer cell lines tested but considering its attenuated expression in U937 cells and its poorly understood role in leukaemia's response to chemotherapeutics, further analysis was done with U937 a pro-monocytic, human myeloid leukaemia cell line.

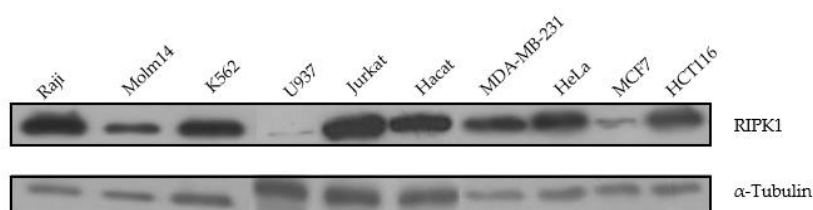


Figure 7. RIPK1 protein expression in several cancer cell lines from whole cellular extract.

U937 cells grown in suspension, and they are characterized by a round shape, short microvilli, and a large radius-shaped nucleus. These monocytic cells have the potential to differentiate into macrophages or dendritic cells in response to various stimuli.

5.2 MC2494 displays context-specific regulation in cancer cell

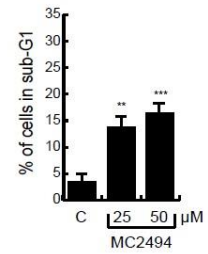
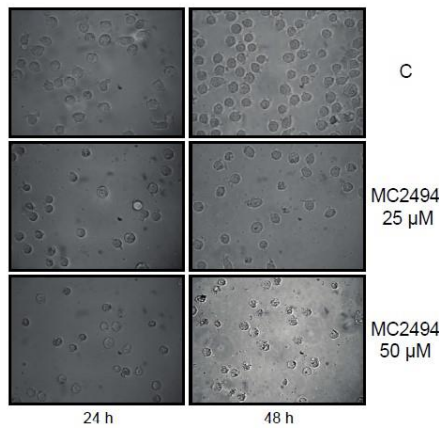
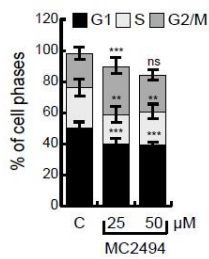
The pan-SIRT inhibitor MC2494 blocks cell proliferation by inducing cell death in a broad panel of cancer cells. In order to identify the potency of the compound in context-specific actions against cancer, we studied its effects on cell cycle distribution in human solid and haematological cancer cells.

Specifically, we evaluated the MC2494 biological activities in a broad panel of breast cancer cells, such as MCF7, triple-negative MDA-MB-231, T47D, and MDA 453 cells; and in a broad panel of leukemia cells such as acute myeloid U937 (M5) and HL60 (M2) cells, and K562 cell line derived from a chronic myeloid leukemia patient expressing B3A2 bcr-abl hybrid gene.

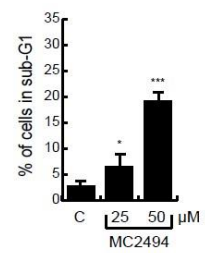
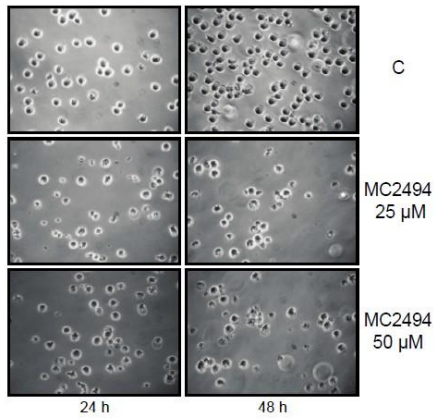
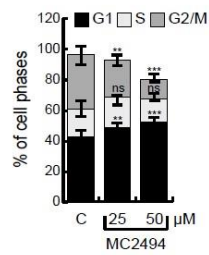
Leukemia cell lines were induced only for 24 h with MC2494 and cell cycle was analysed. In U937 cells, MC2494 determined a robust reduction in G1 phase detectable already at 25 μ M concentration after 24 h of treatment (39.6%), and slight changes in S and G2/M phases (S, 20.6%; G2/M, 29.2%) (Figure 8A left panel).

While MC2494 did not alter cell cycle progression in HL60 cells, in K562 cells we observed an increase in G1 phase already at 25 μM (49.4%), and a reduction in G2/M phase (24.6%). An even greater G2/M phase reduction (12.7%) was observed with the higher concentration of 50 μM (Figure 8B, C left panel). Analysis of the hypodiploid sub-G1 population revealed that U937 and HL60 cells were sensitive to MC2494 treatment already at 25 μM concentration (12.9% and 22.9%, respectively) (Figure 8A, B right panel). In contrast, in K562 cells MC2494 treatment induced an increase in sub-G1 phase (19.4%) only at 50 μM concentration (Figure 8C right panel).

A
U937 cells



C
K562 cells



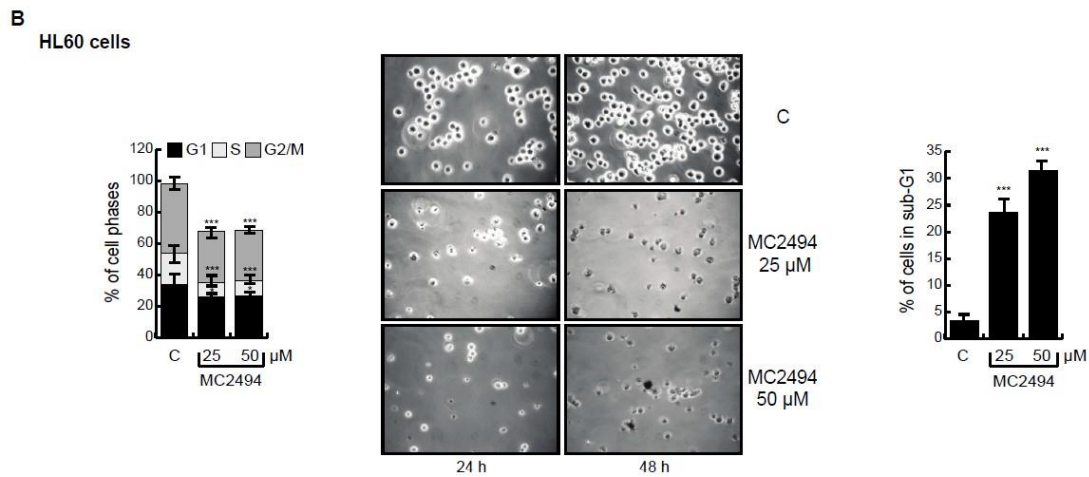


Figure 8. MC2494 affects proliferation in leukemia cancer cell lines. U937, HL60, and K562 cells were treated with MC2494 for 24 h and 48 h at two different concentrations (25 μ M and 50 μ M). Cell cycle analysis (left panels), morphological analysis performed with bright-field light microscopy (40 \times) (middle panels), sub-G1 analysis (right panels). (A) Experiments performed with U937 cells. (B) Experiments performed with HL60 cells. (C) Experiments performed with K562 cells. Graphs show the mean of at least two independent experiments with error bars indicating standard deviation. Values are mean \pm SD of biological triplicates. *** p-value \leq 0.001, ** p-value \leq 0.01, * p-value \leq 0.05, ns p-value $>$ 0.05 vs. control cells.

A different biological effect of MC2494 was observed in breast cancer cell lines, treated for two different time (24-48h). In MCF7 cells, treatment with MC2494 (25 μ M) determined an appreciable G1 phase arrest (60.9%) compared to control cells (51.8%) after 24 h (Figure 9A left panel). Further investigation of MDA-MB-231, MDA 453, and T47D cell lines revealed a reduction in G1 phase and a slight increase in G2/M phase after MC2494 treatment (50 μ M). In MDA-MB-231 cells, the percentage of cells in G1 phase decreased (47.3%) after 24 h of treatment (Figure 9B left panel). A slight effect on G1 phase was observed in T47D cells after 48 h of treatment with MC2494 at both concentrations (25 μ M, 47.6%; 50 μ M, 45.9%) (Figure 10B left panel). Unlike the other cell lines, MDA 453 cells showed a decrease in cell population in G1 phase (48.9%) after 24 h of MC2494 treatment already at the lower concentration of 25 M (Figure 10A left panel). As regards the sub-G1 population, treatment with MC2494 at both concentrations (25 μ M and 50 μ M) induced cell death in T47D cells (8.8% and 8.9%, respectively), and at a final concentration of 50 μ M induced an effect in MCF7 cells (10%) (Figure 9A, right panel and Figure 10B, right panel).

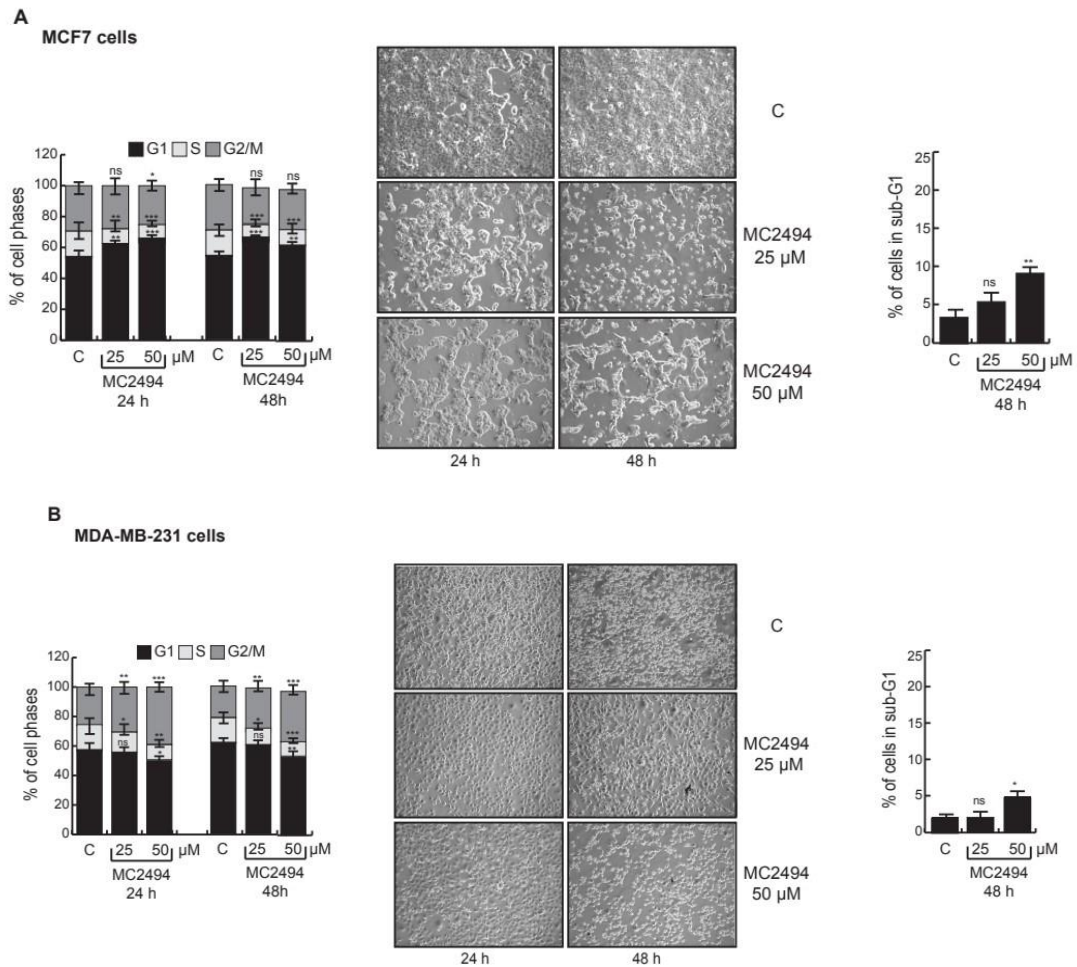


Figure 9. MC2494 affect proliferation in breast cancer MCF7 and MDA-MB-231 cell lines. Both cell lines were treated with MC2494 for 24 h and 48 h at two different concentrations (25 μ M and 50 μ M). Cell cycle analysis (left panels), morphological analysis performed with bright field light microscopy (20X) (middle panels), sub-G1 analysis (right panels). (A) Experiments performed with MCF7 cells. (B) Experiments performed with MDA-MB-231 cells. Graphs show the mean of at least two independent experiments with error bars indicating standard deviation. Values are mean \pm SD of biological triplicates. **** p-value \leq 0.0001, *** p-value \leq 0.001, ** p-value \leq 0.01, * p-value \leq 0.05, ns p-value $>$ 0.05 vs. control cells.

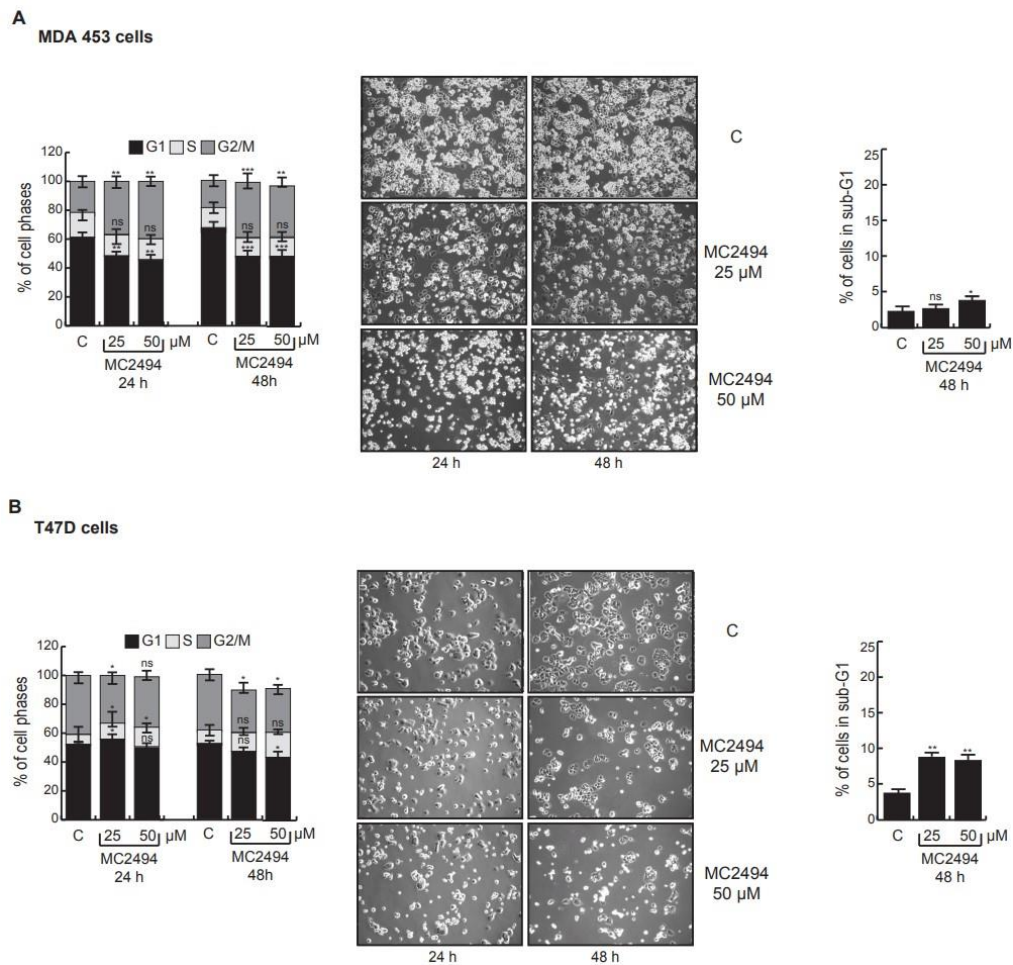


Figure 10. MC2494 affect proliferation in breast cancer MDA 453 and T47D cell lines. Both cell lines were treated with MC2494 for 24 h and 48 h at two different concentrations (25 μ M and 50 μ M). Cell cycle analysis (left panels), morphological analysis performed with bright field light microscopy (20X) (middle panels), sub-G1 analysis (right panels). (A) Experiments performed with MDA 453 cells. (B) Experiments performed with T47D cells. Graphs show the mean of at least two independent experiments with error bars indicating standard deviation. Values are mean \pm SD of biological triplicates. ****p-value \leq 0.0001, ***p-value \leq 0.001, **p-value \leq 0.01, *p-value \leq 0.05, ns p-value $>$ 0.05 vs. control cells.

A robust proliferation arrest and cell death were also detected by morphological analysis performed in all cancer cell lines investigated. Results obtained using bright field light microscopy (20X, breast cancer cells; 40X, leukemia cells) were consistent with the data presented, corroborating the previously reported finding that MC2494 reduces proliferation rate and viability in cancer cell lines (Figures 8, 9, 10). Cell death analyses highlighted that breast cancer cell lines were more resistant to MC2494 induction than leukemia cells.

To confirm sub-G1 data, we also investigated PI intercalation to evaluate dead-cell membrane permeabilization in all cell lines after MC2494 treatment. After PI staining, a strong decrease in living cells was detected already after 24 h of treatment at 50 μ M in MCF7 (15%), MDA-MB-231 (10%), MDA 453 (30%), T47D (20%), U937 (32%), HL60 (25%), and K562 (16%) cells (Figure 11A, B).

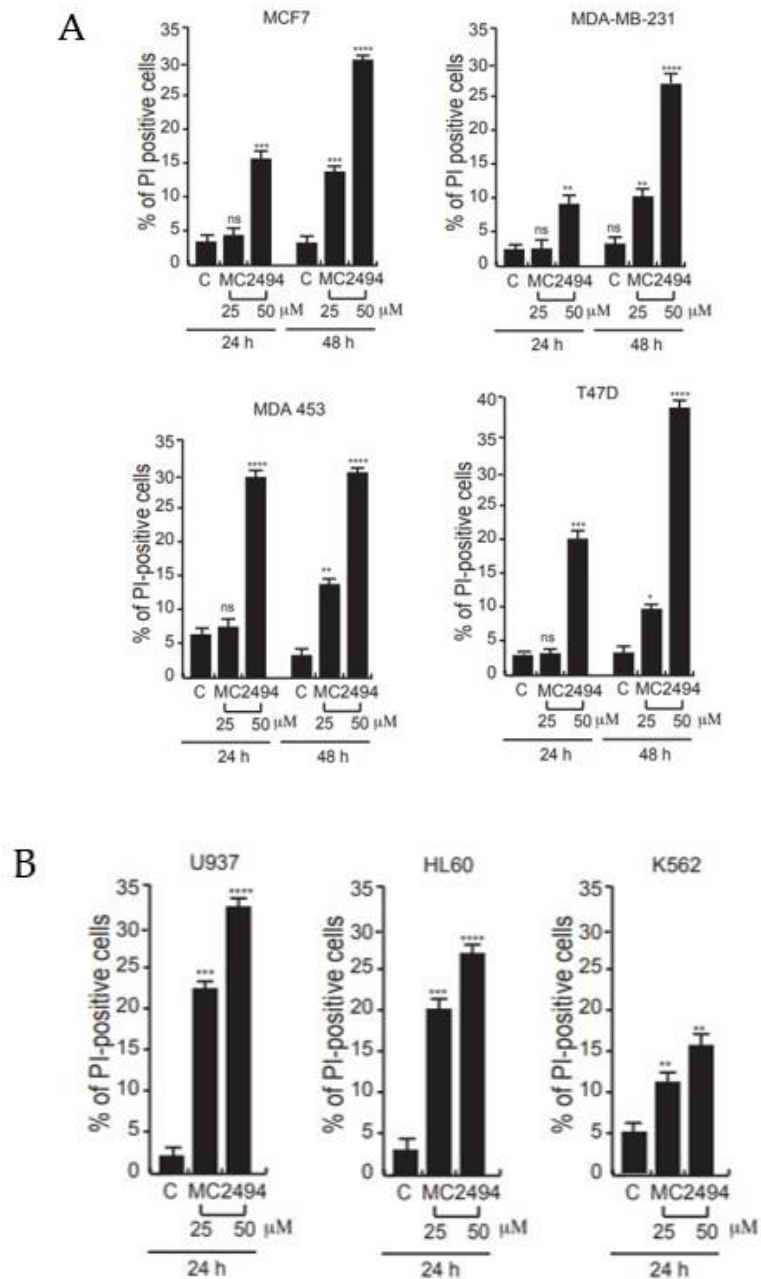
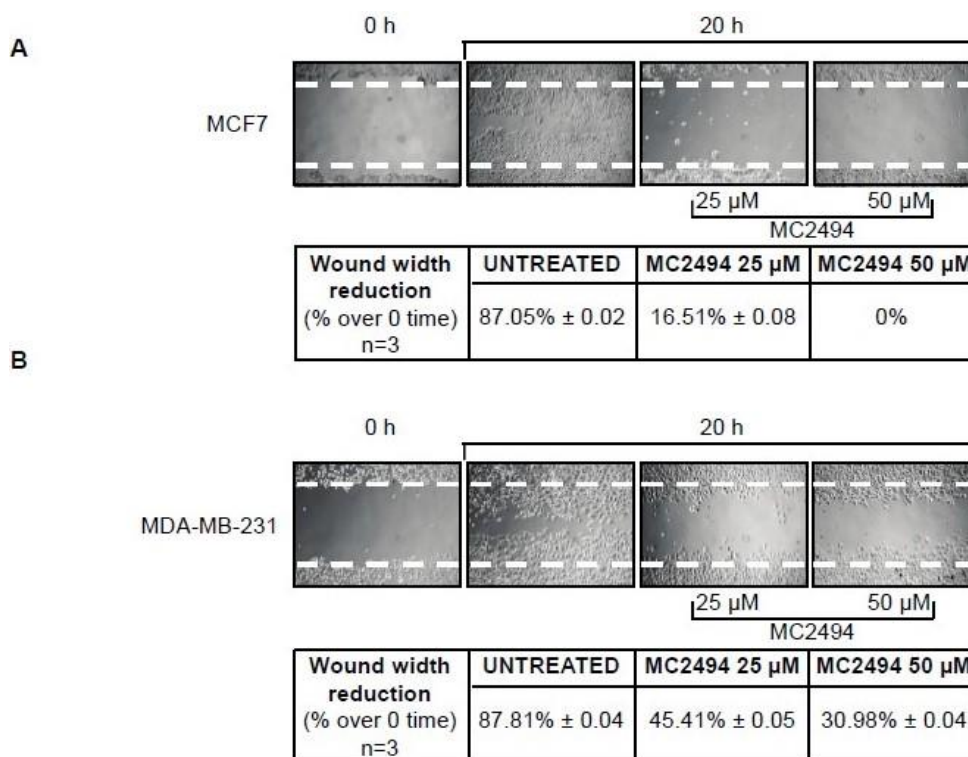


Figure 11. MC2494 induces cell death. (A) PI evaluation in breast cancer cells performed with MC2494 at 25 μ M and 50 μ M concentration after 24 h and 48 h induction. (B) PI evaluation in leukemia cells performed with MC2494 at 25 μ M and 50 μ M concentration after 24 h induction. Graphs show the mean of three independent experiments with error bars indicating standard deviation. Values are mean \pm SD of biological triplicates. ****p-value \leq 0.0001, ***p-value \leq 0.001, **p-value \leq 0.01, *p-value \leq 0.05, ns p-value $>$ 0.05 vs. control cells.

5.3 MC2494 impacts on cancer cell migration

To investigate whether MC2494 affects cell migration, we treated MCF7 and MDA-MB-231 cells at two different concentrations (25 μ M and 50 μ M) for 20 h and performed wound-healing experiments. Representative images from one experiment were captured by contrast-phase microscopy (Figure 12A, B). The wound width from different experiments was analysed as a reduction in wound area compared to 0 time. Our results show that a significant number of cells migrated to the wound area in cycling cells and that MC2494 already inhibited cell migration at a concentration of 25 μ M in both MCF7 and MDA-MB-231 cells. To further assess the effect of MC2494 on cell migration, K562 cells were treated with MC2494 at 25 μ M and 50 μ M for 36 h and analysed with Boyden's chamber system (Figure 12C, D). MC2494 treatment at 50 μ M inhibited by 2-fold the number of migrating K562 cells. U937 cells were not used for these experiments due to their high sensitivity to MC2494 treatment in terms of cell death. To confirm these data, conditioned medium from MCF7 cells was added in the lower chamber of the Transwell system. Several studies showed that the addition of conditioned medium promotes cell migration. In these experimental conditions, we observed a drastic reduction in the number of migrating K562 cells after 36 h of MC2494 treatment (Figure 12C, D). To confirm this finding, Western blot analysis performed for two metalloproteinases (MMP2 and MMP9) involved in cell migration revealed that together with the block of proliferation an accumulation of the metalloproteinase inactive forms (pro-MMP2 and pro-MMP9) occurred (Figure 12E). These findings indicate that SIRT inhibition mediated by MC2494 has a functional role in cancer cell migration.



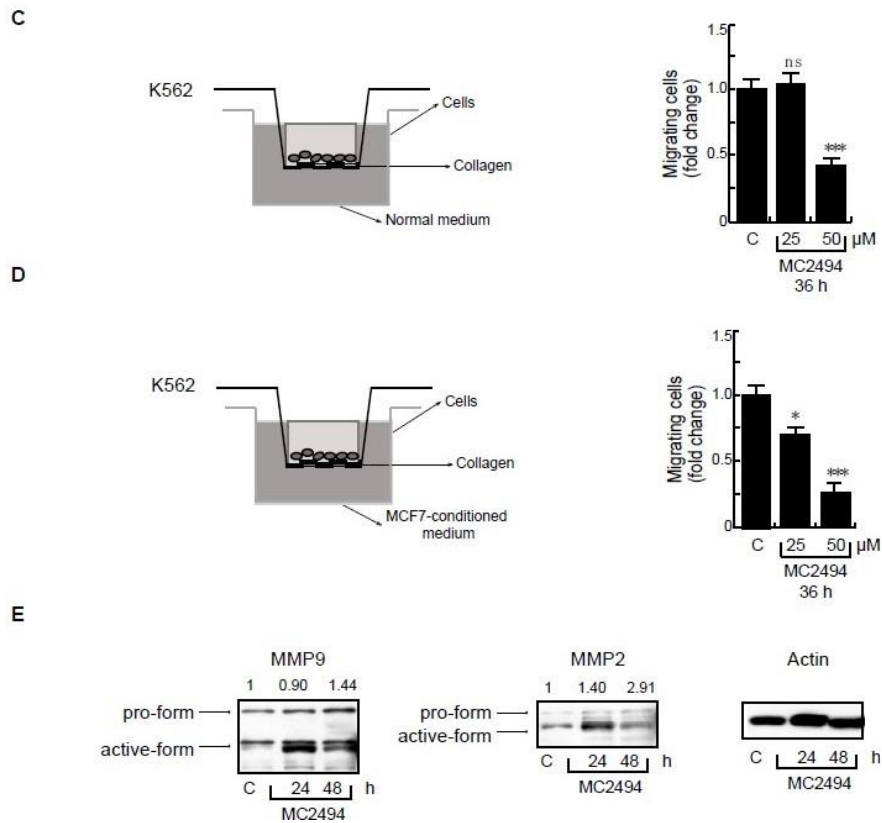


Figure 12. MC2494 affects cell migration. (A) Wound-healing assay performed in MCF7 cells at indicated times and concentrations. (B) Wound-healing assay performed in MDA-MB-231 cells at indicated times and concentrations. (C) Migration analysis using Boyden's chamber system performed in K562 cells. (D) Migration analysis using Boyden's chamber system performed in K562 cells. (D) Migration analysis using Boyden's chamber system performed in K562 cells after treatment with conditioned medium. (E) Western blot analysis of MMP2 and MMP9. Actin was used as control for equal loading. Values are mean \pm SD of biological triplicates. *** p-value \leq 0.001, * p-value \leq 0.05, ns p-value $>$ 0.05 vs. control cells.

5.4 Study of cell death in U937 cell line

We previously reported that treatment with MC2494 determines a strong increase in cell death in many cancer cell lines [68]. This interesting biological data strength the antitumor potential of this compound and open to an in-depth characterization of cell death events. Considering the difficulties of treatment in acute leukemia, we thought to better define the cell death observed in U937 cells after MC2494 treatment at 50 μ M for 24 h. To this aim, Live & Dead cell assay and Hoechst staining were performed. The result demonstrates a clear difference when the observed live (green peak) and dead (red peak) cells were analysed by flow cytometry after treatment with MC2494 for 24 h (Figure 13).

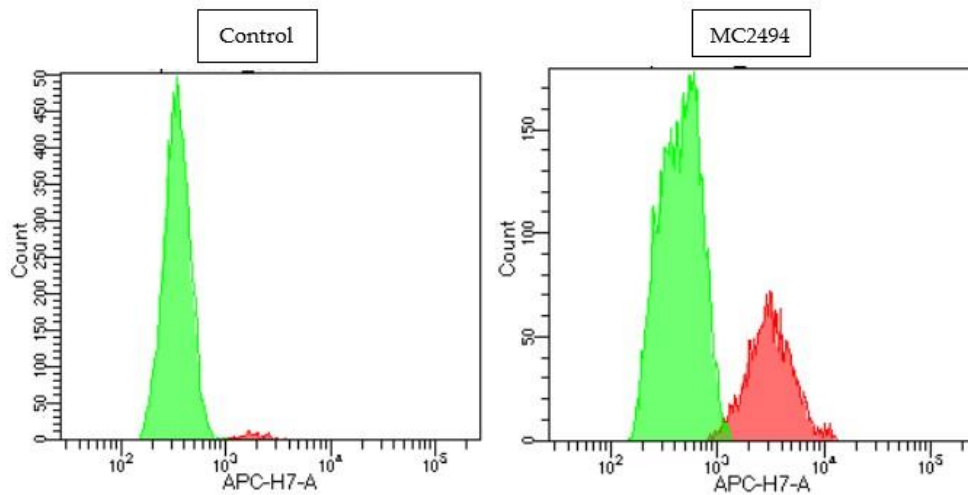


Figure 13. MC2494 affects cell death in U937 cells. Fluorescent staining with BD Horizon Fixable Viability Stain 780.

Immunofluorescence experiments, after nuclei staining, clearly highlighted pycnotic nuclei, condensation, and chromatin fragmentation, confirming the reduction of cell proliferation with regulated cell death events (Figure 14).

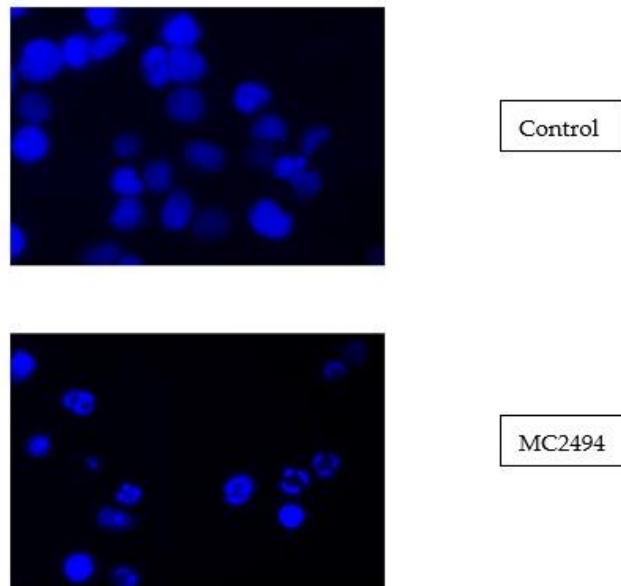


Figure 14. Hoechst coloration. Objective lenses 20X. Graphs show the mean of at least three independent experiments with error bars indicating standard deviation. Values are mean \pm SD of biological triplicates. ****p-value \leq 0.0001, ***p-value \leq 0.001, **p-value \leq 0.01, *p-value \leq 0.05, ns p-value $>$ 0.05 vs. control cells.

The double staining Annexin V/PI carried out in U937 cells treated with MC2494 at 50 μ M for different times of induction (6–24 h), strength the observed data. Early and late-stage apoptotic cells were detected and

analysed by FACS. After 16 h and 24 h of induction, an increase in apoptotic population at early stage (5.39% and 12.40%, respectively) and at late stage (8.99% and 12.13%, respectively) was observed (Figure 15).

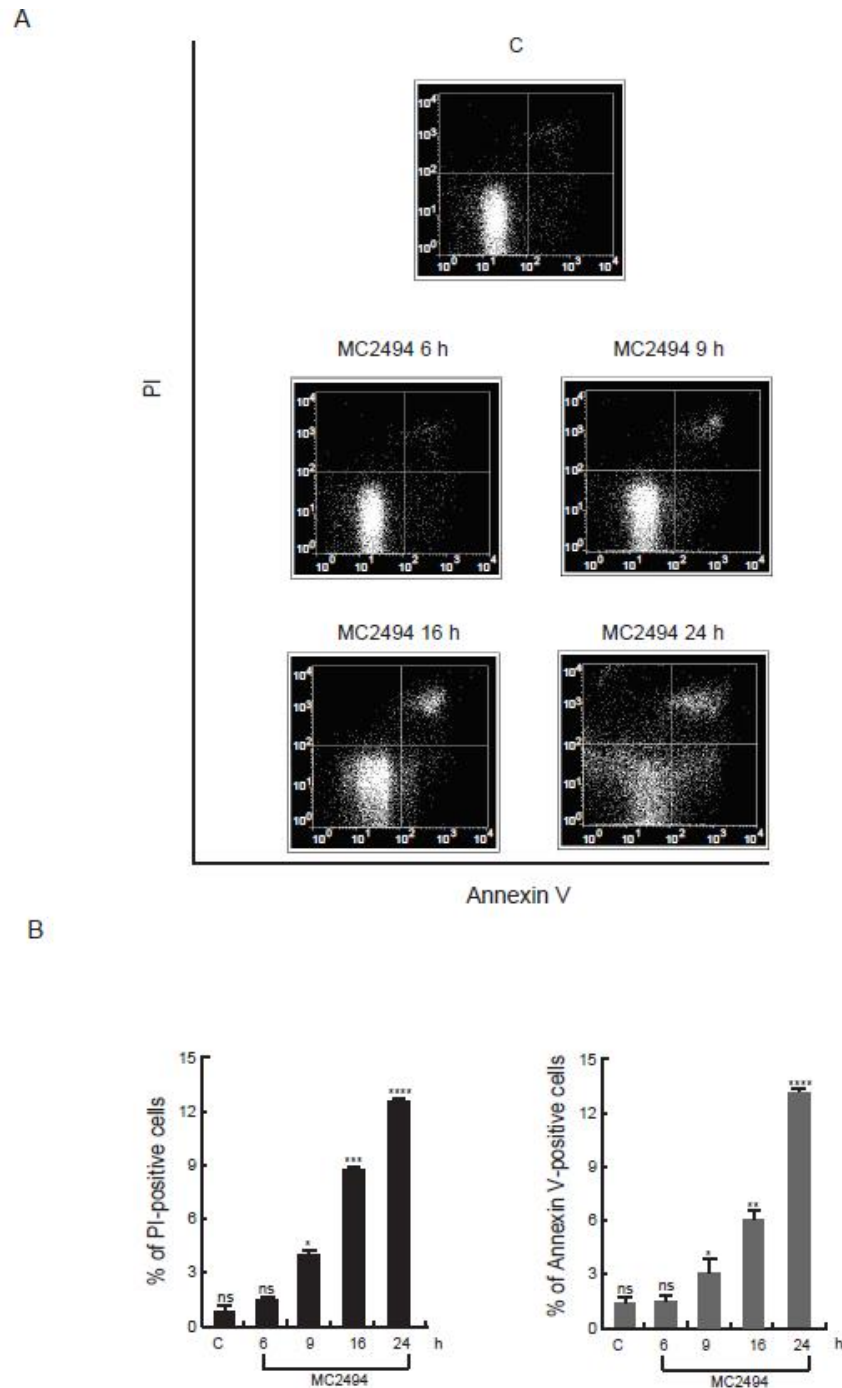
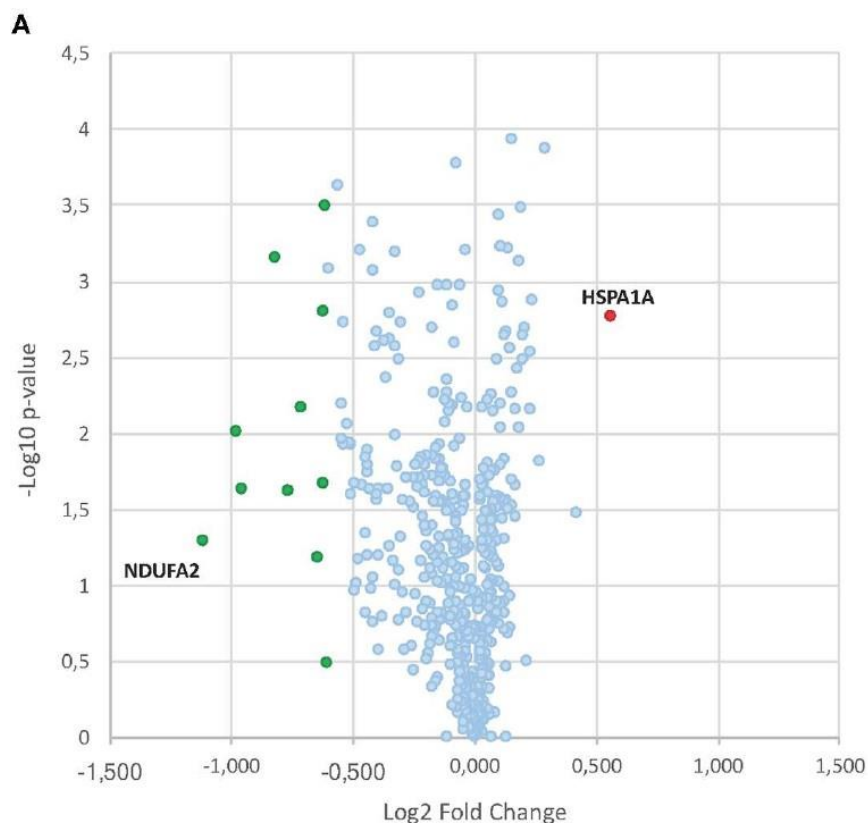


Figure 15. Study of apoptotic events. Annexin V/PI assays were performed in U937 cells with MC2494 at 50 μ M concentration at indicated times of induction. (A) Density plots of Annexin V/PI evaluation. (B) Annexin V/PI analysis; Left panel: PI-positive cells; Right panel: Annexin V-positive cells. Graphs show the mean of three independent experiments with error bars indicating standard deviation. Values are mean \pm SD of biological triplicates. ****p-value \leq 0.0001, ***p-value \leq 0.001, **p-value \leq 0.01, *p-value \leq 0.05, ns p-value $>$ 0.05 vs. control cells

5.6 MC2494 regulates mitochondrial function in U937 cell line

Mitochondria are complex organelles that influence cancer initiation, growth, survival and metastasis, and have a central role in apoptotic cell death [69]. In addition, these organelles are essential for TNF-induced necroptosis in several cell types [70]. Given dynamic role of mitochondria, many studies are focusing on the involvement of mitochondria in cancer development and progression [71]. We previously demonstrated that the pan-SIRTi MC2494 causes an increase in ROS production, a consistent dissipation of mitochondrial membrane potential (MMP), and activation of mitochondrial apoptotic pathway [1]. Hence, in this project we investigated the effects of MC2494 treatment on mitochondria and identified potential connections between MC2494-mediated cellular response and mitochondrial dysfunction. The relative complexity of the mitochondrial proteome requires the use of high-throughput methodologies for the large-scale profiling of key pathways involved in mitochondrial dysfunction. To gain a greater understanding of the molecular effects of MC2494 on mitochondrial proteome, we adopted an advanced quantitative proteomic approach based on TMT isobaric labeling and nano-liquid chromatography coupled with high resolution MS/MS analysis. A very small fraction (about 2.4%) of identified proteins was found differentially expressed ($0.6 \geq \text{fold change} \geq 1.5$) in MC2494 treated compared to untreated U937 cells (Figure 16A). A specific subset of down-regulated proteins was associated with respiratory electron transport and related pathways (Figure 16B).



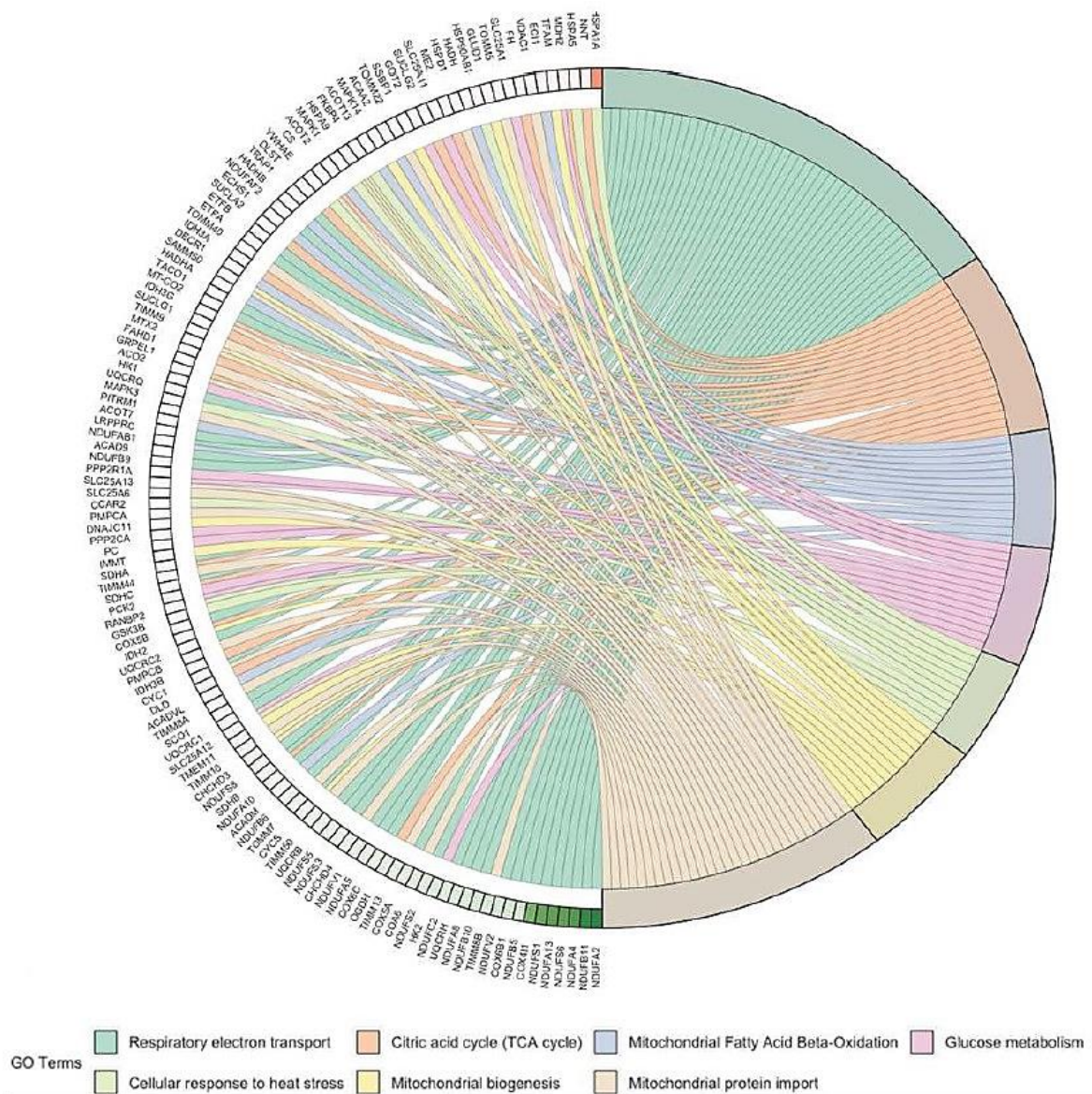


Figure 16. (A) Volcano plot obtained from TMT-based quantitative proteomic analysis of MC2494-treated vs. untreated U937 cells. Each point represents the difference in expression (log₂ fold change) between MC2494-treated vs. untreated samples plotted against the -log₁₀ p-value. Identified proteins with no changes in their regulation level are in light blue. Up- and down-regulated proteins (0.6 ≥ fold change ≥ 1.5) are shown in red and green, respectively. (B) GOChord plot showing relationships between selected representative biological process GO terms and related proteins identified by nanoLC-MS/MS analysis. The red and green color scale within the plot refers to protein log₂ fold change values.

Growing scientific interest is focusing on mitochondrial function in terms of the key role of energy homeostasis in cell viability, and mitochondria biogenesis. Based on proteomic results we further investigated the peroxisome proliferator activated receptor γ coactivator 1 (PGC1) family that has an important function in regulating mitochondrial metabolism [72]. We studied the expression of PGC1 α , which is involved in mitochondrial biogenesis.

Interestingly, in U937 cells we observed a significant and consistent decrease in mRNA levels already after 3 h of MC2494 treatment (Figure 17A). In line with this result, Western blot analysis of PGC1 α and PGC1 β , both members of the PGC1 family, showed a similar decrease in protein expression with MC2494 treatment at 50 μ M for the indicated times (Figure 17B).

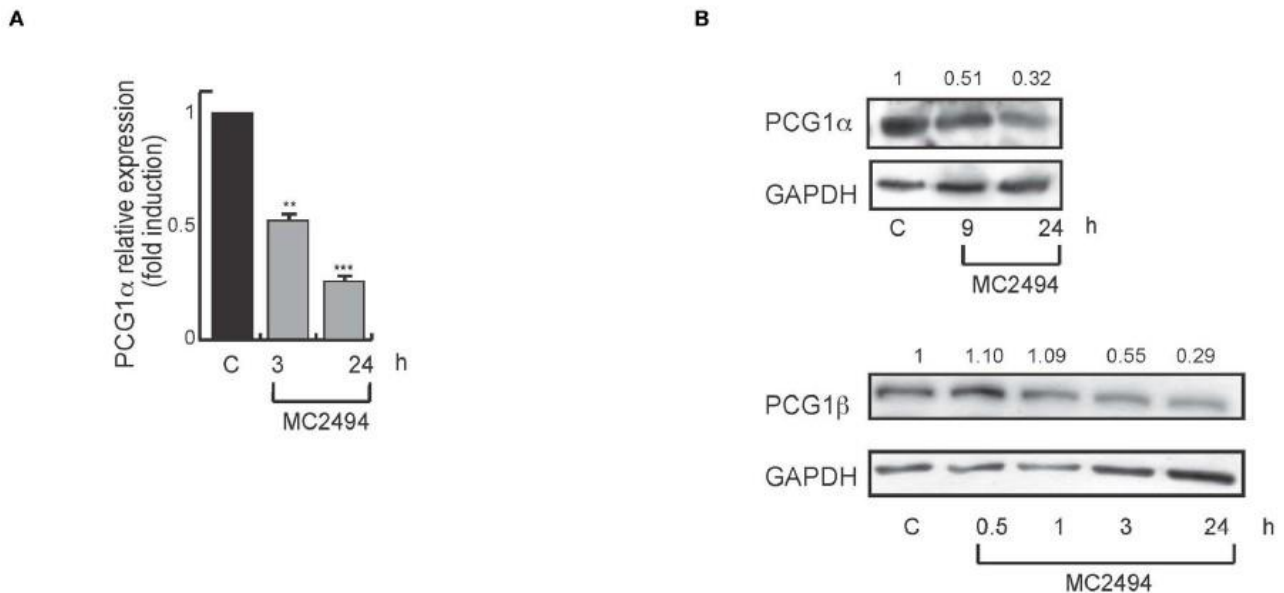


Figure 17. **(A)** mRNA evaluation of PGC1 α in U937 cells treated with MC2494 at 50 μ M concentration for 3 and 24 h. U937 cells were treated with MC2494 for the indicated times at 50 μ M concentration. GAPDH was used as control for equal loading. Graphs show the mean of at least 2 independent experiments with error bars indicating standard deviation. **(B)** Top panel, western blot analysis of PGC1 α ; bottom panel western blot analysis of PGC1 β . U937 cells were treated with MC2494 at 50 μ M concentration for indicated times. Numbers on Western blot indicate the results of densitometry analysis, performed using the Image J Gel Analysis tool.

To assess whether the reduction in PGC1 α/β levels coincides with a loss of mitochondria, we studied the total mitochondrial content in U937 cells after MC2494 treatment. In control cells, immunofluorescence microscopy revealed the presence of intact mitochondria mostly localized in the cytoplasm. Already after 3 h of MC2494 induction, and more evident after 16 h of treatment, an accumulation of fragmented short mitochondria resulting from mitochondrial dysfunction caused by MC2494-induced cell death was observed (Figure 18). The total disruption of mitochondria consistent with a higher percentage of MC2494-mediated cell death was detected after 24 h of induction.

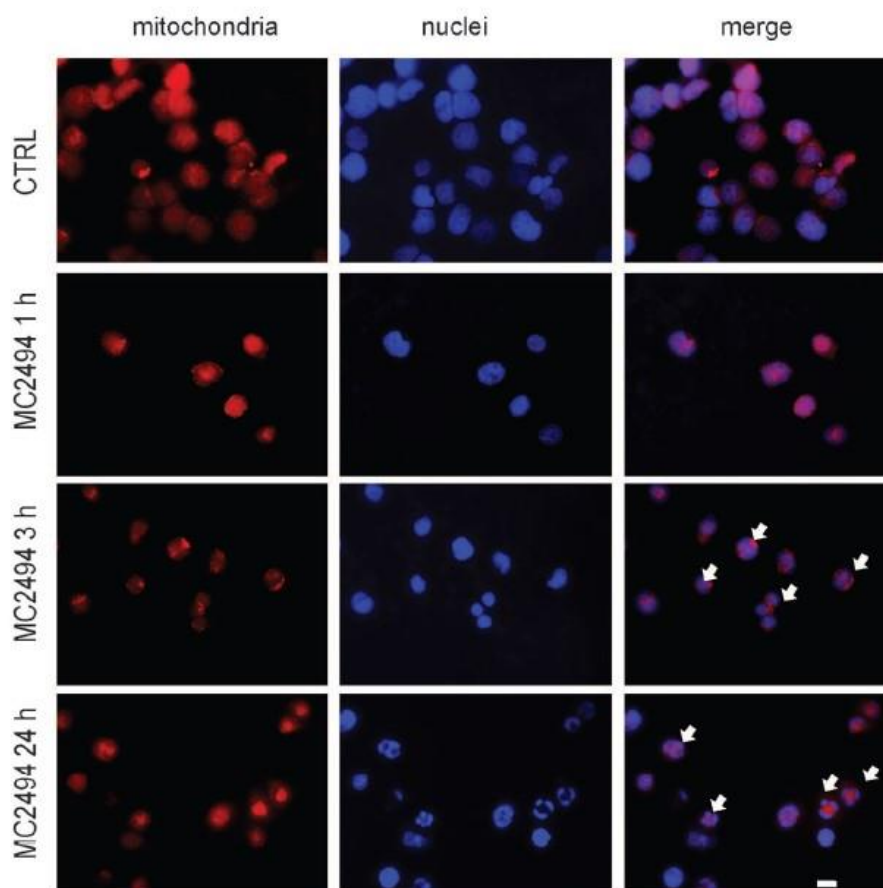


Figure 18. Immunofluorescence analysis. MitoTracker Orange staining for cells untreated or treated for the indicated times with MC2494. Images representative of 3 different experiments captured by immunofluorescence microscope show staining of mitochondria (red) and nuclei (blue). Bar, 10 μ M. Arrows denote the presence of fragmented mitochondria and nuclei after 3 and 16 h of MC2494 treatment.

We found that MC2494 has a general effect on mitochondrial functions and may therefore orchestrate cell response to metabolic stress, interfering with cancer promotion and progression. Therefore, our findings identify a close interaction between MC2494-mediated cellular response and mitochondrial dysfunction. Given that most cancers rely on anaerobic glycolysis for ATP production, the block of mitochondrial function mediated by MC2494 may play a pivotal role in several tumours modulating redox and energy homeostasis, transcriptional regulation, and cell death.

5.5 Several biological processes enriched after MC2494 treatment

To further investigate the effect of the pan-SIRTi at molecular level, whole-transcriptome sequencing by RNA-Seq of control and treated U937 cells with MC2494 50 μ M for 24 h provides robust information to identify the regulated genes in order to facilitate the understanding of biological processes affected by the treatment. The data analysis heat map of DESeq2 shows that replicates of each genotype cluster together and, to confirm,

principal component analysis suggests that the two conditions cluster far from each other (PC1 96% variance) (Figure 19 A, B).

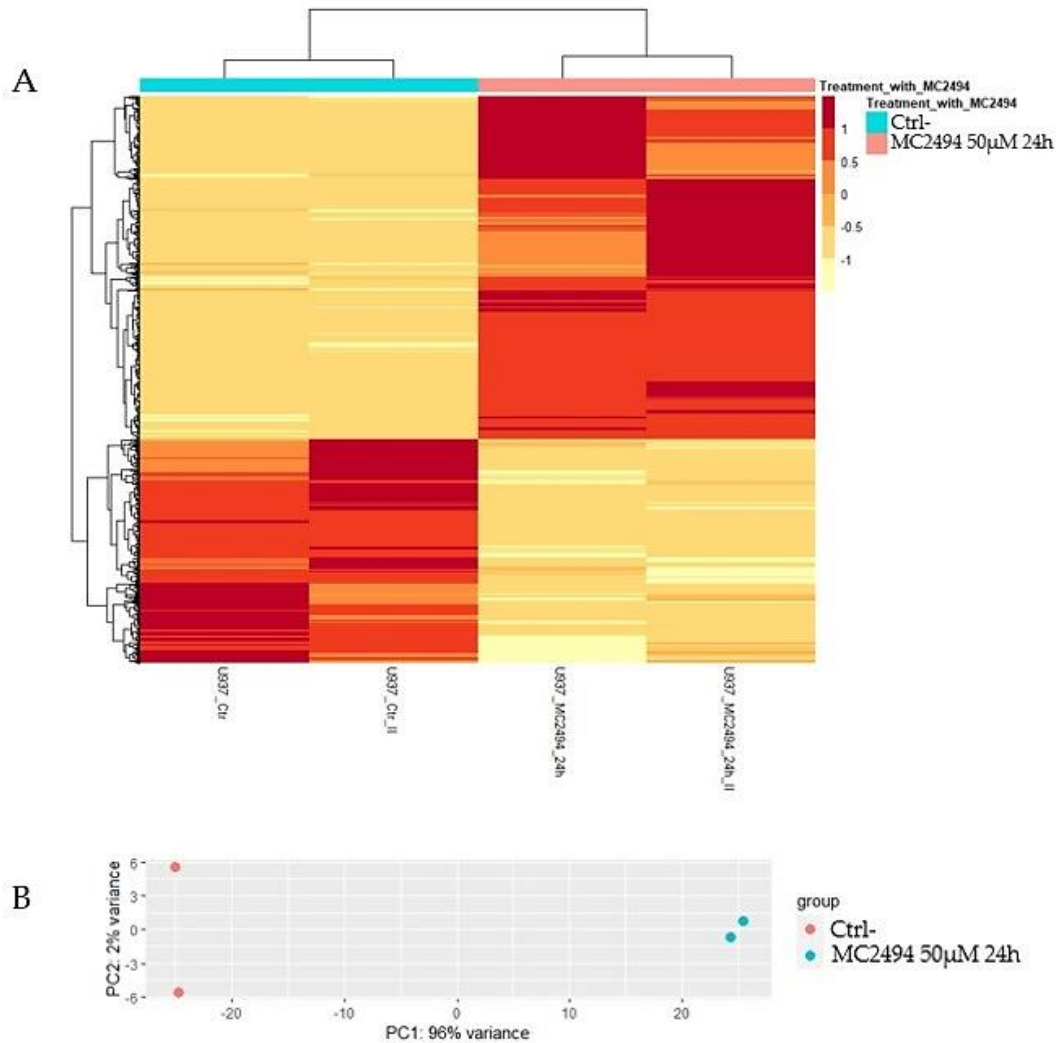


Figure 19. Clustered expression heatmap of the normalized counts of the DE genes. (A) Heat map; (B) Principal component analysis.

For visualizing and identifying gene expression datasets from the two different conditions, we used MA plot, a 2-dimensional (2D) scatter plot in which genes with similar expression values in both normal and treated samples will cluster around $M=0$ value while points away from $M=0$ line indicate genes with significant expression (Figure 20).

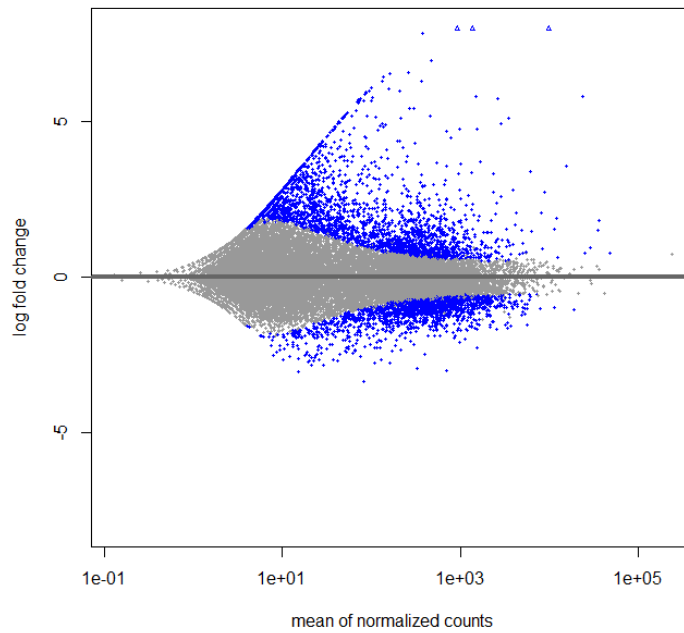


Figure 20. MA plot shows the log₂ fold changes attributable to a given variable over the mean of normalized counts for all the samples in the dataset. Compared to the control, above line 0 (in blue) the up-regulated genes in the treatment, while below line 0 (in blue) the down-regulated genes in the treatment.

Since MA plot does not consider statistical measures (p values or adjusted p values) we used Volcano plot to indicate genes with statistically significant differences between normal *vs* treated (Figure 21).

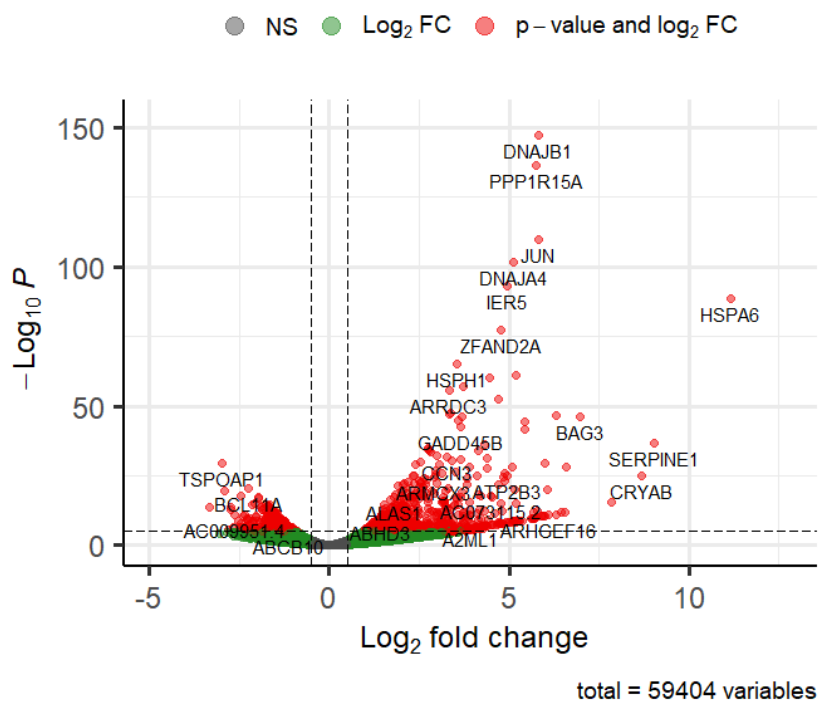


Figure 21. Volcano plot showing DE genes. To the right of zero DE genes by the treatment.

Furthermore, obtaining a list of DE genes is only the starting point for gaining biological knowledge about experimental systems or understanding molecular mechanisms. To understand the biological context of DE genes, pathway enrichment analysis follows. Gene Ontology (GO) analysis using TOPPGENE tool system (<https://toppgene.cchmc.org/>) on differentially expressed genes (2462 up, 1603 down) was performed. Considering >1 log2FoldChange up-regulated genes, the enriched biological processes, grouped in the list below, include unfolded protein response (UPR), regulation of cell death, regulation of protein ubiquitination and positive regulation of NF- κ B transcription factor activity. For the down-regulated DE genes, the enriched biological processes mostly regard the cell cycle regulation and the response to DNA damage stimuli followed by chromatin organization (Figure 22).

Biological processes induced upon treatment

ID	Name	pValue	Bonferroni	
1	GO:0006986	response to unfolded protein	4.633E-25	4.304E-21
2	GO:0035966	response to topologically incorrect protein	1.157E-24	1.075E-20
3	GO:0034620	cellular response to unfolded protein	7.706E-19	7.158E-15
4	GO:0035967	cellular response to topologically incorrect protein	4.162E-18	3.866E-14
5	GO:0034976	response to endoplasmic reticulum stress	2.943E-17	2.734E-13
6	GO:0030968	endoplasmic reticulum unfolded protein response	2.918E-16	2.710E-12
7	GO:0042981	regulation of apoptotic process	8.657E-14	8.041E-10
8	GO:0043067	regulation of programmed cell death	2.175E-13	2.020E-9
9	GO:0043066	negative regulation of apoptotic process	3.833E-13	3.561E-9
10	GO:0010941	regulation of cell death	1.422E-12	1.320E-8
11	GO:0043069	negative regulation of programmed cell death	1.588E-12	1.475E-8
12	GO:0060548	negative regulation of cell death	2.315E-11	2.151E-7
13	GO:0036498	IRE1-mediated unfolded protein response	5.230E-11	4.858E-7
14	GO:1901698	response to nitrogen compound	5.788E-11	5.376E-7
15	GO:0010243	response to organonitrogen compound	1.644E-10	1.527E-6
16	GO:0080134	regulation of response to stress	4.663E-10	4.331E-6
17	GO:0080135	regulation of cellular response to stress	7.876E-10	7.315E-6
18	GO:0031329	regulation of cellular catabolic process	2.389E-9	2.219E-5
19	GO:1905897	regulation of response to endoplasmic reticulum stress	2.719E-9	2.525E-5
20	GO:0010498	proteasomal protein catabolic process	2.921E-9	2.713E-5
21	GO:0006457	protein folding	2.929E-9	2.721E-5
22	GO:0006508	proteolysis	4.286E-9	3.981E-5
23	GO:0031396	regulation of protein ubiquitination	5.965E-9	5.541E-5
24	GO:0009894	regulation of catabolic process	6.358E-9	5.905E-5
25	GO:0051092	positive regulation of NF- κ B transcription factor activity	6.944E-9	6.450E-5

Biological processes repressed upon treatment

ID	Name	pValue	Bonferroni	
1	GO:0051276	chromosome organization	2.559E-16	2.141E-12
2	GO:0022402	cell cycle process	4.080E-13	3.413E-9
3	GO:0006325	chromatin organization	2.102E-12	1.759E-8
4	GO:0002520	immune system development	7.036E-12	5.886E-8
5	GO:0006259	DNA metabolic process	7.667E-12	6.414E-8
6	GO:0001775	cell activation	9.577E-12	8.012E-8
7	GO:0044772	mitotic cell cycle phase transition	1.247E-11	1.043E-7
8	GO:0000082	G1/S transition of mitotic cell cycle	1.979E-11	1.656E-7
9	GO:0030097	hemopoiesis	3.397E-11	2.842E-7
10	GO:0044770	cell cycle phase transition	5.390E-11	4.509E-7
11	GO:0048285	organelle fission	5.542E-11	4.636E-7
12	GO:0044843	cell cycle G1/S phase transition	6.121E-11	5.120E-7
13	GO:0000278	mitotic cell cycle	6.805E-11	5.693E-7
14	GO:0140014	mitotic nuclear division	6.805E-11	5.693E-7
15	GO:1903047	mitotic cell cycle process	6.805E-11	5.693E-7
16	GO:0048534	hematopoietic or lymphoid organ development	7.044E-11	5.893E-7
17	GO:0000280	nuclear division	1.440E-10	1.205E-6
18	GO:0045321	leukocyte activation	2.461E-10	2.058E-6
19	GO:0002521	leukocyte differentiation	3.711E-10	3.105E-6
20	GO:0006913	nucleocytoplasmic transport	4.491E-10	3.757E-6
21	GO:0051169	nuclear transport	6.101E-10	5.104E-6
22	GO:0032259	methylation	1.493E-9	1.249E-5
23	GO:0016569	covalent chromatin modification	1.674E-9	1.401E-5
24	GO:0006974	cellular response to DNA damage stimulus	2.020E-9	1.690E-5
25	GO:0043414	macromolecule methylation	2.592E-9	2.168E-5

Figure 22. GO analysis. Enriched GO categories in a set of significantly down- and up-regulated genes when comparing control samples to MC2494 treated samples. Cutoff 0,05.

As expected, among the up- and down-regulated DE genes, the ones most affected by modulation after treatment are those of the cell death and cell cycle signaling pathways, respectively, thus confirming the action of MC2494 as an antitumor agent in leukemia, which aims to restore the correct execution of altered and silenced cellular pathways. Furthermore, the DE genes of protein folding and of the ubiquitination process (also involved in modulation) are very interesting as they play an essential role in the maintenance of cellular homeostasis.

5.7 MC2494 regulates different biological aspects over time

To better understand the mechanistic insights and to define the potential biomedical effects of the pan-SIRTi, we decided to make a time-course experiment with a fixed dose of 50µM. During the time, the action of MC2494 induced strong proliferation arrest compared to the control (Figure 23). These data strongly imply wide-ranging antiproliferative effects.

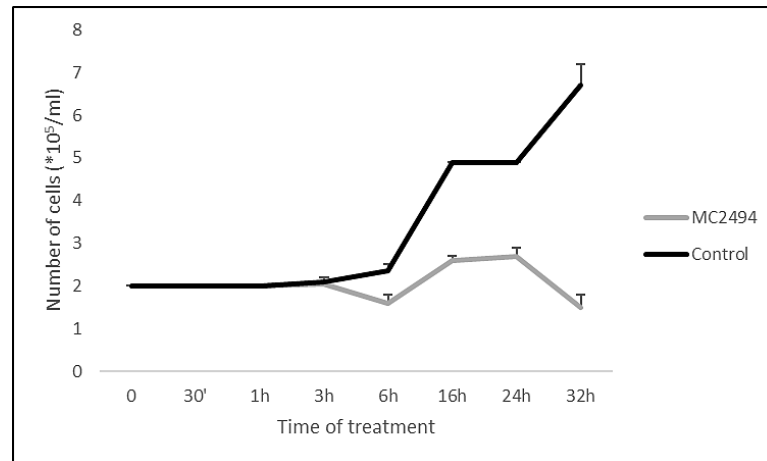


Figure 23. MC2494 affects proliferation in U937 cells at different times of treatment.

The percentage of PI positive cells showed a greater increase at the longer treatment times of 16 h and 24 h (9,35% and 30.05%, respectively) (Figure 24A) and the hypodiploid sub-G1 peak on fixed cells identified a strong increase in sub-G1 peak, displaying a higher percentage starting from 16 h of treatment (27%) (Figure 24B).

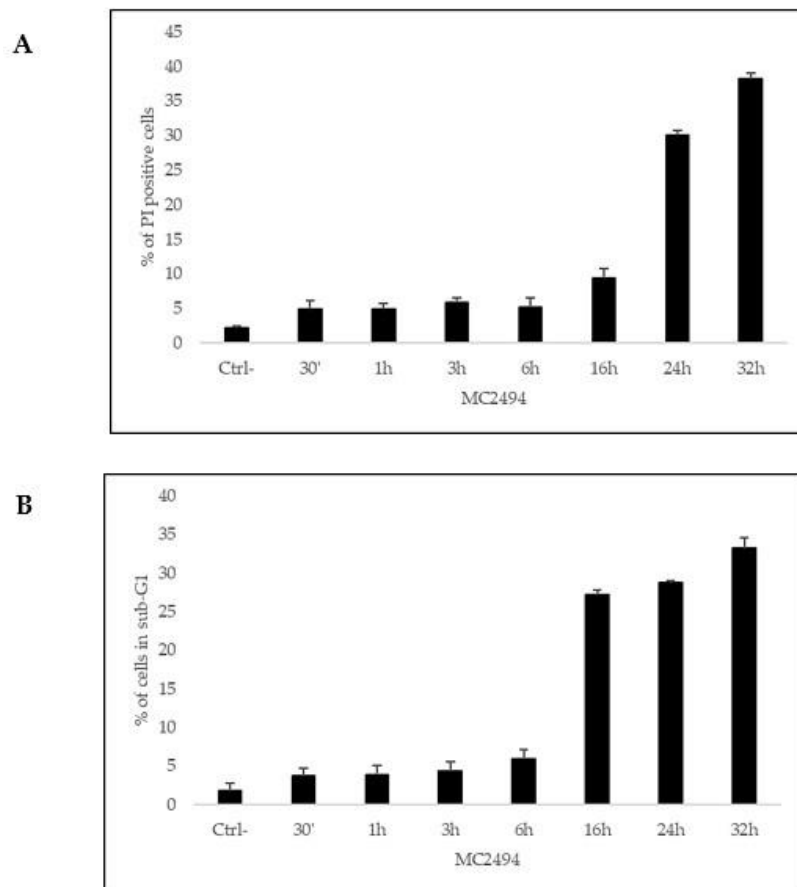


Figure 24. Effects of MC2494 on (A) propidium iodide (PI) incorporation and (B) hypodiploid sub-G1 phases. U937 cells were treated with the compound at 50 μ M for several time points.

For what concern cell cycle progression, the analysis showed that the treatment alters the cell cycle progression determining a reduction in G1 phase, a slight change in S phase and a robust reduction in G2/M phases detectable especially after 16 h till 32 h of treatment (Figure 25).

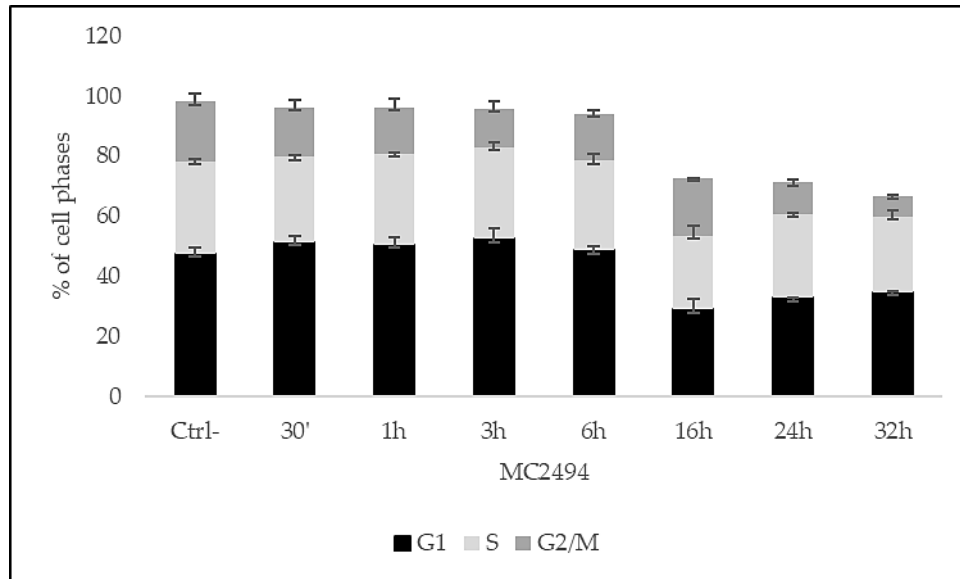


Figure 25. Effect of MC2494 on cell cycle regulation. U937 were treated with MC2494 for the indicated times at 50 μ M.

Taken together these results indicate that MC2494 exerts its biological anticancer effects by the regulation of cell cycle, and the induction of cell death already at early time of treatment (16h).

5.8 MC2494 modulates RIPK1

Previous data reported that RIPK1 is part of a molecular complex in which deacetylases, acetyltransferases and kinases work together to determine the induction of cell death. Moreover, the activity of MC2494 results in a modulation of this complex via a regulatory role for acetylation of RIPK1-mediated cell death [1]. To better understand the not well characterized role of RIPK1 in leukemia, we evaluated its protein expression in U937 cells after the treatment at 50 μ M concentration for different times of induction (0.5-32 h). Already at early time of treatment (9 h) it was possible to observe a decrement in RIPK1 protein expression, effect more evident after 24 and 32 h (Figure 26). Based on this observation, some proteins involved in necrosome formation such as RIPK3 and MLKL were investigated, but no substantial modulation was observed for these two proteins after MC2494 treatment (Figure 26).

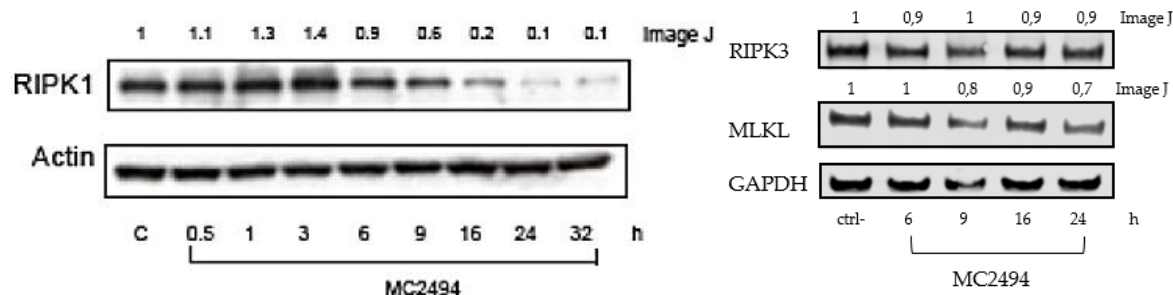


Figure 26. MC2494 regulates necrosome. Western blot analysis of RIPK1, RIPK3 and MLKL. Actin and GAPDH were used as loading controls. Numbers on Western blot indicate the result of densitometry analysis, performed using the Image J Gel Analysis tool.

To strengthen the observed data and to better clarify the function of MC2494, U937 cells were treated with Nec-1, a selective RIPK1 inhibitor for different times (9-24 h) at 50 μ M of concentration. Surprisingly, Nec-1 did not affect necrosome complex formation (Figure 27). These results led us to hypothesize a possible enzymatic role of MC2494 as a RIPK1 inhibitor.

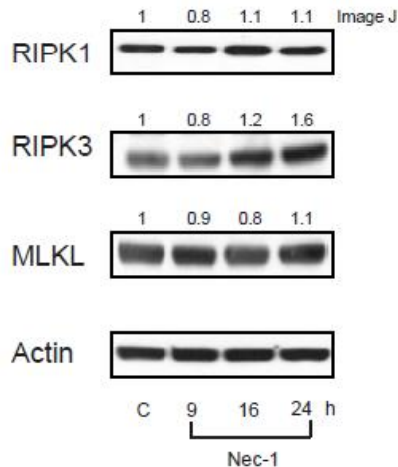


Figure 27. Necrosome components evaluation after Nec-1 treatment. Western blot analysis of RIPK1, RIPK3 and MLKL. Actin was used as loading control. Numbers on Western blot indicate the result of densitometry analysis, performed using the Image J Gel Analysis tool.

To this aim, with a computational support was created a docked model of “how” MC2494 binds RIPK1, starting from reported data for GNE684, a newly characterized RIPK1 inhibitor, that binds RIPK1 to the same hydrophobic pocket and in a similar conformation to Nec-1.

In this model, MC2494 binds to an inactive conformation of RIPK1, like Nec-1, GNE684 and other type III kinase inhibitors, with Asp156 and Leu157 of the DLG motif (commonly DFG in other kinases) in the “out”

conformation (Figure 28). The computed interaction energy as assessed by MVD scoring function (-132.7) is comparable to that measured for GNE684 (-148.4), suggesting that MC2494 may act as a RIPK1 inhibitor with comparable efficacy to GNE684.

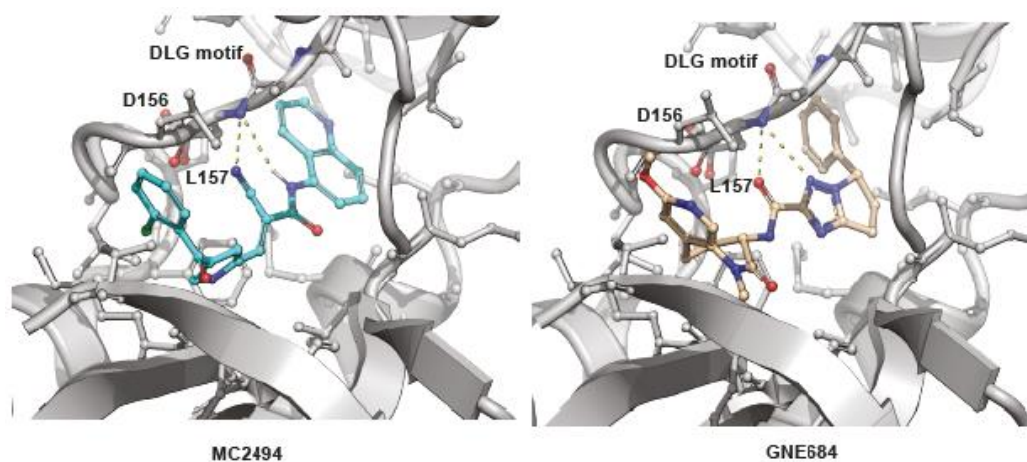


Figure 28. Cartoon representation of the docked pose of MC2494 (cyan sticks – Left Panel) and B) GNE684 (pink sticks – Right Panel) into the experimentally determined complex with RIP1 (PDB: 6NYH). Nitrogen and oxygen atoms are colored blue and red, respectively. Polar interactions between the compounds and the protein moiety are shown in yellow dashed lines.

To define a possible role of MC2494 as kinase inhibitor, we next tested its enzymatic activity by performing in vitro kinase assay using recombinant RIPK1 (Figure 29). The experiment was conducted by evaluating the percentage of luminescence emitted after treatment with MC2494 compared to Nec-1 and GSK3145095. Remarkably, we observed a clear inhibitory effect of Nec-1 and GSK3145095 reaching 54% and 96% reduction in RIPK1 enzymatic activity, respectively. Importantly, MC2494 had no effect on RIPK1 activity. This result suggests that unlike the two potent RIPK1 inhibitors, MC2494 is not a direct RIPK1 inhibitor.

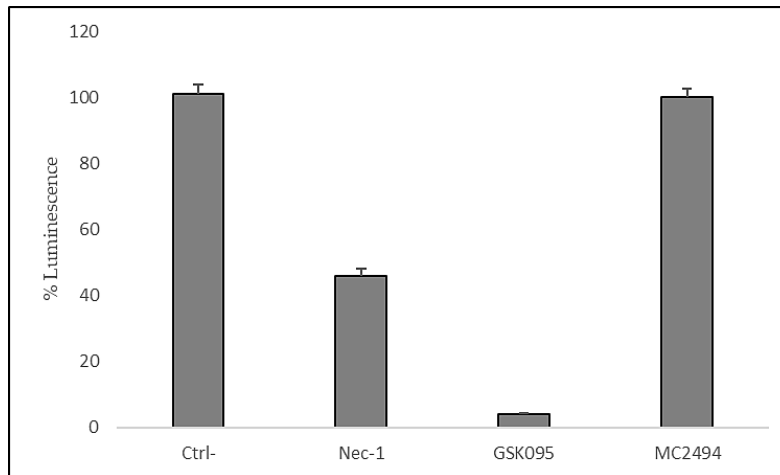


Figure 29. MC2494 doesn't act as direct RIPK1 kinase inhibitor. Enzymatic activities were measured by ATP consumption using ADP-Glo kinase assays. The compounds were used at 50 μ M concentration. To avoid the possible interference of the compounds with the luminescence reaction we presented the results in the absence of active kinase. Results are shown as a percentage relative to the ADP-Glo luminescence reaction and are the mean \pm SEM of three independent kinase assays (n = 3).

Although MC2494-RIPK1 modulation was confirmed in U937 cells, we applied a cellular thermal shift assay (CETSA) to follow compound-induced protein interaction changes. It is interesting to note that the presence of MC2494 does not protect RIPK1 from the thermal degradation thus biologically validating the enzymatic data (Figure 30).

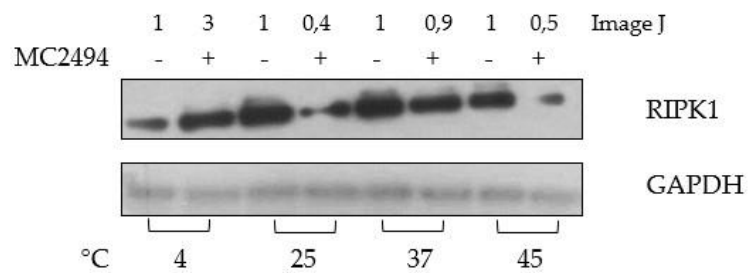


Figure 30. CETSA assay. Western blot analysis for RIPK1 evaluation after MC2494 at 50 μ M treatment. GAPDH was used as loading control. Numbers on Western blot indicate the result of densitometry analysis, performed using the Image J Gel Analysis tool.

6. DISCUSSION

Cell death has a great impact in the regulation of physiological and pathological phenomena. Cancer cells learn to prevent apoptotic mechanisms by modifying the functions of anti- or pro-apoptotic proteins through post-translational modifications [73]. A very promising prospect that led to the approval, by the American *Food and Drug Administration*, is the use of drugs with epigenetic activity, able to restore the correct functioning of some genes of fundamental importance for cellular activity. A particularly interesting group of compounds is that of class III histone deacetylase inhibitors, sirtuins. The well-discussed role of sirtuins in the carcinogenesis process makes them a specific and selective pharmacological target [3]. In the experimental work carried out, the attention was focused on the biological effects of a compound, MC2494, a previously identified and characterized pan-sirtuins inhibitor [1]. The mechanism of action is fully in line with the concept of epigenetic therapy, which aims to restore the correct execution of altered and silenced cellular pathways. Data obtained via analysis of cell proliferation and apoptosis induced by MC2494 corroborated the activity of MC2494, warranting further studies.

To better investigate the antiproliferative mechanism(s) of MC2494 in different systems, we studied its action in a broad panel of cancer cell line, haematological (leukemia) and solid (breast) cancers. Our study revealed that, among the three leukemia cell lines used, U937 cells were more sensitive than HL60 and K562 cells to MC2494-induced cell death, already at the lower concentration of 25 μ M. In contrast, breast cancer cell lines were generally more resistant to MC2494 treatment, which resulted in a low percentage of sub-G1 populations. Interestingly, MCF7 cells were more sensitive than all other breast cancer cell lines, suggesting the potential activation of different biological pathways via SIRT inhibition. Of note, results obtained in different cell lines from sub-G1 evaluation and PI staining following MC2494 treatment showed different responses, particularly in breast cancer cells (which were positive to PI staining but displayed a low sub-G1 fraction). This observation suggests that the modulation of early as well as late apoptotic pathways varies in a context-dependent manner. Further studies are needed to contextualize the role of the MC2494 in different types of cancer. Cell cycle and sub-G1 phases were affected by SIRT inhibition induced by MC2494, with leukemia U937 and breast-cancer MCF7 cells exhibiting a different regulation. These data strengthen the context-specific action of SIRT inhibition even at the level of cell cycle regulation, suggesting that the antiproliferative effects of MC2494 might be obtained by activating different regulatory pathways of cell cycle progression.

The deregulation of cell death in tumorigenesis is a well understood hallmark of cancer. Among the new characterized RCD, necroptosis is deregulated in many types of cancer, showing an high potential as therapeutic targets for the treatment of all tumours resistant to chemotherapeutic agents or inducers of apoptosis [15,31]. While the function for RIPK3 and MLKL have been highlighted, few (to no) evidence has been underlined for RIPK1 in leukemogenesis. To this aim we addressed our experiments to better understand the involvement of RIPK1 in leukaemia cells, exploring the effect of MC2494 on the necrosome components.

At protein level the induction with MC2494 causes a substantial decrease in the expression of only one necrosome component, RIPK1. This (de)regulation has been observed exclusively at protein level; indeed, exploring DE genes from RNA-seq data analysis, neither RIPK1 nor RIPK3 were differently regulated after MC2494 treatment. In addition, despite the predicted ability of MC2494 to bind RIPK1 in its enzymatic pocket, a specific kinase assay showed that MC2494 is not a direct inhibitor of RIPK1, data supported by CETSA assay, revealing the lack of a direct interaction between the compound and the protein.

Taking together these data supported the idea of the activation of a non-canonical necroptotic pathway, in which RIPK1 is complexed to other proteins responsible of its degradation. Considering that unfolded protein response (UPR) and ubiquitination processes are some of the main biological processes promoting protein degradation, we looked for these biological processes from RNA-seq data. After treatment a global upregulation of these gene were observed.

It is already known that the alternative necroptosis mechanism does not require RIPK1 and is induced by receptors other than TNFR1, such as TLR3 and DAI. Downstream of these receptors, the RHIM domain necessary to recruit and activate RIPK3 is provided by TRIF or by the DAI itself.

These evidence, together with the upregulation only at genomic level of the last interactor of necrosome death complex, MLKL, led us to hypothesize that RIPK1 is misfolded and degraded via ubiquitination, by the action of MC2494, probably due to the activation of UPR in the endoplasmic reticulum (ER) under stress.

Considering the accumulation of unfolded or misfolded proteins in the ER lumen mediate UPR effector proteins triggering, MC2494 may have a pivotal role in the activation of this molecular response, leading to RIPK1 degradation, silencing of survival related pathway, and activation of non-canonical PCD signaling pathway [74].

7. CONCLUSION

In conclusion, our study highlights the importance in the use of epigenetic compounds, able of blocking cancer growth by selective activation of a specific cell death pathway. Targeting necrosome may lead to a reprogramming of cell death and cell fate. Modulating/detecting RIPK1-complex might be crucial to overcome the deregulation of cell death in cancer and to improve the sensitivity to the anti-tumour therapies. The explanation of "how" RIPK1 regulates the outcomes of the different cell death pathways and their involvement in leukemogenesis, will be useful to define how it can be a target for pharmaceutical attempts, increasing and reinforcing the already well discussed concept of personalized therapy.

Furthermore, the work provides the basis for a future developing of tool of new drugs based on the structure-active relationship study.

A further investigation will be necessary to better clarify the activated molecular pathway driven by MC2494 that is responsible of RIPK1 degradation in acute myeloid leukaemia. After this study it will possibly hypothesize to expands the current views of the therapy, making it more efficacy thanks to a low toxicity and more specificity increasing the therapeutic index and reducing the development of therapy resistance.

8. MATERIAL AND METHODS

8.1 Cell Line and Culture Conditions

U937, HL-60, K562 cells were purchased from DSMZ. MDA-MB-231, MDA 453, MCF-7 and T47D cells were from Cell Bank Interlab Cell Line Collection. All cell lines were grown following standard protocols. The human pro-monocytic myeloid leukemia cell line U937, the Promyeoloblasts HL60 and the lymphoblasts K562 were maintained in suspension culture in Roswell Park Memorial Institute (RPMI) 1640 medium supplemented with L-glutamine (0.3 g/L), 10% (v/v) heat-inactivated fetal bovine serum (FB-1345), and antibiotics [1% (v/v) penicillin–streptomycin]. The epithelial, human breast cancer cell lines MDA-MB-231 and MCF7 were from Cell Bank Interlab Cell Line Collection. They were cultured in Dulbecco's modified Eagle's medium (DMEM) supplemented with L-glutamine (0.3 g/L), 10% (v/v) heat-inactivated fetal bovine serum (FB-1345), and antibiotics [1% (v/v) penicillin–streptomycin]. The cells were grown at 37°C in 5% CO₂ in a humidified atmosphere and subcultured every day or 2nd day.

8.2 Ligands

MC2494 (and derivatives), Nec-1 (Sigma) and GSK3145095 were dissolved in DMSO (Sigma) and used at 50 μM. MC2494, its derivatives and GSK3145095 were synthesized by University Sapienza, Rome, Italy.

8.3 Protein extraction

Cell pellets were washed in PBS and suspended in lysis buffer (50 mM Tris-HCl pH 7.4, 150 mM NaCl, 1% NP-40, 10 mM NaF, 1mM phenylmethylsulfonyl fluoride) and protease inhibitor. The lysis reaction was carried out for 15 mins at 4 °C and centrifuged at 13,000 rpm for 30 min at 4 °C. Protein concentration was quantified by Bradford assay (Bio-Rad).

8.4 Western blot

Fifty μg of proteins was loaded onto 10% polyacrylamide gels and transferred to nitrocellulose membrane using a transfer apparatus according to the manufacturer's protocols (Bio-Rad). The nitrocellulose filters were stained with Ponceau red (Sigma) as additional control for equal loading then the membrane was blocked with 5% non-fat milk in TBST (10 mM Tris pH 8.0, 150 mM NaCl, 0.5% TWEEN 20) for 60 min, the membrane was washed three times with TBST and incubated with antibodies. Detection was performed with an Enhanced chemiluminescence (ECL) system (EuroClone) according to the manufacturer's protocol. Western blots were normalized through densitometry analysis, performed using the Image J Gel Analysis tool.

8.5 Antibodies

RIPK1 was purchased from BD Biosciences (BD 610459), RIPK3 (SC374639) and Actin (SC8432) were purchased from Santa Cruz, MLKL (D2I6N #14993) was purchased from Cell Signaling and GAPDH (E-AB-20059) was purchased from Elabscience, PGC1a (ab191838) and PGC1b (ab176328) were both purchased from Abcam.

8.6 Morphological Analysis

Morphological analysis for MCF7 and MDA-MB-231 cancer cell lines was performed using bright field light microscopy (20X). For U937, HL60 and K562 cancer cell lines, the analysis was performed using bright-field light microscopy (40X).

8.7 Wound-Scratch Assay

For wound-scratch assay, 1.5×10^5 cells were seeded in a 24-well plate. Cells were wounded using 10 μ L sterile pipette tips. Cells were washed with PBS and then untreated or treated for the indicated time in the absence or presence of 50 μ M of MC2494. Cytosine arabinoside (Sigma-Aldrich) at 50 μ M (final concentration) was included in the cell medium to avoid cell proliferation. Different fields were analyzed using a DM IRB inverted microscope (Leica) equipped with an N-Plan 10x objective (Leica) and Application Suite Software (Leica). Contrast-phase images, representative of at least three different experiments, were captured using a DC200 camera (Leica). The wound gap was calculated using Image J software and expressed as a percentage of the decrease in wound area.

8.8 Boyden's Chamber Assay

Boyden's chamber assay was performed using collagen-I from rat-tail (BD Biosciences)-coated Transwells with 8 μ m polycarbonate membrane (Corning). Cycling cells were plated in the upper chamber at 5×10^4 per well in 150 μ L complete medium. When indicated, MCF-7 conditioned medium was added to the lower chambers. Cells were allowed to migrate for 36 h in a humidified incubator at 37°C with 5% CO₂ in the absence or presence of the compound added to the upper and lower chambers at the indicated concentrations.

After 36 h, non-migrating cells from the membrane upper surface were removed using a sterile cotton swab. The polycarbonate membranes were fixed for 20 min in 4% paraformaldehyde, stained with Hoechst, removed with forceps from the companion chamber and mounted. Migrating cells from at least 30 fields/each membrane were counted as described [38], using a DMBL fluorescent microscope (Leica), equipped with an HCPL Fluotar 20X objective. Data are representative of three different experiments.

8.9 Mitochondria Content

U937 cells were treated with MC2494 for different times (0.5–24 h). After treatment, MitoTracker Orange dye (Invitrogen#M7510) at a final concentration of 10 μ M was added for 30min. After 2 washes in PBS, cellular pellets were suspended in PBS containing propidium iodide (0.5 μ g/mL) and analyzed with FACS CELESTA. Data analysis was performed using CellQuest software (BD Biosciences).

8.10 Mitochondria Labeling

Labeling solution prepared with MitoTracker Orange dye (Invitrogen) at a final concentration of 1 μ M was added to medium and cells were incubated for 45min. After 3 washes with PBS, cells were fixed in 4% paraformaldehyde (Sigma-Aldrich #P6148) for 20min. After 2 washes with PBS, nuclei were stained using Hoechst 33258 (Sigma-Aldrich #94403) at a final concentration of 1 μ g/mL. Finally, coverslips were inverted and mounted in Mowiol (Calbiochem #475904100). Fields were observed using a DMBL Leica fluorescence microscope equipped with HCX PL Fluotar Apo 63X oil objectives. Images representative of 3 different experiments were captured with a DC480 camera (Leica) and acquired using Application Suite (Leica) software.

8.11 Immunofluorescence Microscopy

U937 cells were cultured and grown on coverslips in 12-well plates. After MC2494 treatment, cells were fixed in methanol for 10min at -20°C and blocked with BSA (2%) in TBST for 1 h. Blocked cells were stained with anti-PGC1 α diluted 1:100 in PBS overnight. The day after, coverslips were washed 3 times with PBS-BSA and incubated with anti-rabbit Texas Red-conjugated secondary antibody (diluted 1:400; Jackson Laboratories) for 1 h at room temperature. Nuclei were counterstained with DAPI (10 μ g/mL; Molecular Probes #D1306), extensively washed with PBS-BSA, and mounted in Vectashield mounting medium (Vector Laboratories #H-1000-10). Fields were observed using a DMBL Leica fluorescence microscope equipped with HCX PL Fluotar Apo 63X oil objectives. Images representative of 3 different experiments were acquired and captured with a DC480 camera (Leica) using Application Suite (Leica) software.

8.12 Cell Cycle and Cell Death Analysis

For cell cycle analyses, cells were plated (2 * 10⁵ cells/mL) and after stimulation were harvested, centrifuged at 1200 rpm for 5 min, and resuspended in 500 μ L of a hypotonic solution containing 1X PBS, 0.1% sodium citrate, 0.1% NP-40, RNAase A, and 50 mg/mL PI. Cell death was studied by evaluating hypodiploid sub-G1 peak on fixed cells and PI incorporation on live cells to assess DNA fragmentation (late apoptotic event) and dead-cell membrane permeabilization (early apoptotic event), respectively. For sub-G1 evaluation, samples were prepared as described above. For PI evaluation, cells were plated (2 * 10⁵ cells/mL) and stimulated for the required times. After stimulation, cells were harvested, centrifuged at 1200 rpm for 5 min, and resuspended

in 500 μ L 1X PBS and 0.2 mg/mL PI. The results were acquired on a FACS CELESTA flow cytometer system (BD Biosciences). Each experiment was performed in biological triplicates and values expressed as mean \pm standard deviation.

8.13 Living Cell Image Detection

U937 cells were plated in 48 wells 2×10^5 cells/mL and induced with MC2494 at 50 μ M. After 24 h, the cells were treated with Hoechst Stain solution (B-Bridge) to evaluate the living cells and were analysed by Cytation 5 Cell Imaging Multi-Mode Reader (BioTeK).

8.14 Annexin V Staining

Annexin V evaluation was performed as suggested by the supplier (Dojindo). Briefly, cells were suspended in Annexin V binding solution at the concentration of 1×10^6 cells/mL, 5 μ L of fluorescein isothiocyanate-conjugated Annexin V and 5 μ L PI were added to 100 μ L cellular suspension transferred into a new tube. Reaction was carried out for 15 min at room temperature. The results were acquired on a FACS CELESTA (BD Biosciences). Graphs show the experimental results of biological triplicates.

8.15 Live & Dead assay

BD Horizon™ Fixable Viability Stain 780 (FVS780) is useful for discrimination of viable from non-viable mammalian cells in multicolor flow cytometric applications. $1 - 10 \times 10^6$ cells/ml were washed one time with PBS and resuspended in PBS with 1 μ L of BD Horizon™ Fixable Viability 780 Stock Solution and vortexed. Reaction was carried out for 10-15 min at room temperature. The results were acquired on a FACS CELESTA (BD Biosciences). BD Horizon™ Fixable Viability 780 is excited by the red laser and has a fluorescence emission maximum of 780nm. Graphs show the experimental results of biological triplicates.

8.16 ADP-Glo Kinase assay

ADP-Glo Kinase Assay is a luminescent kinase assay that measures ADP formed from a kinase reaction; ADP is converted into ATP, which is converted into light by Ultra-Glo Luciferase (Promega). The luminescent signal positively correlates with ADP amount and kinase activity. Briefly, for the kinase reaction, the required amount of recombinant human RIPK1 has been incubated in kinase assay buffer (50 mM HEPES pH 7.5, 50 mM NaCl, 30 mM MgCl₂, 4mM DTT, 0.5 mg/mL BSA, and 0.02% CHAPS) at room temperature in the presence or absence of the compounds. To convert ATP consumption into light production, a 2:2:1 (kinase assay reaction:ADP-Glo reagent:kinase detection reagent) ratio of the kit's components was used. The reaction was carried out for 40 minutes at room temperature. Luminescence was measured during 1 s reads with a microplate-reading luminometer.

8.17 CETSA assay

U937 cells were harvested and washed twice with PBS after treatment with MC2494 (50 mmol/L) and an equal amount of DMSO, as control, for 1 hour. The respective samples were suspended in PBS (1 mL), divided into aliquots (100 μ L), and heated at different temperatures (25°C–37°C–44°C–53°C–57°C) for 3 minutes by Thermo Mixer (Eppendorf), followed by cooling for 3 minutes at 4°C. After incubation, lysis buffer (100 μ L) was added to the samples and incubated for 15 minutes. The samples were then centrifuged at 13,000 rpm for 30 minutes at 4°C, the supernatant was removed, and protein concentration was determined using a Bradford assay (Bio-Rad). Of the total protein extract, 20 mg was loaded on 10%SDS-PAGE, and Western blot analysis was performed. The antibody used was RIPK1.

8.18 Sample preparation for proteomic analysis

For proteomic analysis, MC2494-treated with MC2494 at 50 μ M and untreated U937 cells were lysed in ice-cold lysis buffer (100mM triethylammonium bicarbonate [TEAB, #90114, Thermo Scientific], 1% SDS) and disrupted by two cycles of sonication at 20% amplitude for 30 sec on ice. Lysates were cleared by centrifugation at 16,000 \times g for 15min at 4°C. Supernatants were transferred into new tubes and treated with 1 unit of RQ1 DNase (#M6101, Promega) for 1 h at room temperature. Protein concentration was determined using Pierce BCA Protein Assay Kit (#23225, Thermo Scientific). For each condition, equal amounts of proteins (100 μ g in 100 μ L of 100mM TEAB) were reduced with 10mM tris-(2-carboxyethyl)-phosphine (TCEP part of TMT 10plex kit, #90113, Thermo Scientific) for 1 h at 55°C and alkylated with 18mM iodoacetamide (part of TMT 10plex kit, #90113, Thermo Scientific) by incubating samples for 30min at room temperature in the dark. Proteins were then precipitated overnight by adding 6 volumes of pre-chilled acetone (#15623200, Honeywell Riedel de Haen, Fisher Scientific). Following centrifugation at 8,000 \times g for 10 min at 4°C, protein pellets were resuspended in 100 μ L of 100mM TEAB, digested with trypsin (#90057, Thermo Scientific), and labeled with the following tandem mass tag (TMT, TMT 10plex kit, #90113, Thermo Scientific) isobaric tags using 126 and 127N tags for MC2494-treated and untreated U937 cells, respectively. TMT labeled samples were then mixed and diluted in 2% TFA (#28904, Thermo Scientific) to a final concentration of 0.5 μ g/ μ L for liquid chromatography coupled to tandem mass spectrometry (LC-MS/MS) analysis.

8.19 High-Resolution NanoLC-Tandem Mass Spectrometry

Aliquots of TMT-labeled peptides (2.5 μ g) were analysed by high-resolution nanoscale liquid chromatography coupled to tandem mass spectrometry (nanoLC-MS/MS) using a Q-Exactive Orbitrap mass spectrometer.

8.20 Protein identification and quantitation

For data processing, the acquired raw files were analysed with Thermo Scientific Proteome Discoverer 2.1 software using the SEQUEST HT search engine. The higher-energy collisional dissociation MS/MS spectra

were searched against the Homo sapiens database (release 2019_11, 20380 entries). Mass tolerances were set to 10 ppm and 0.02 Da for precursor and fragment ions, respectively. Oxidation of methionine (+15.995 Da) was set as dynamic modification. Carbamidomethylation of cysteine (+57.021 Da) and the TMT label on lysines and the N-terminus (229.1629) were set as static modifications. False discovery rates (FDRs) for peptide spectral matches were calculated and filtered using the Percolator node in Proteome Discoverer run with the following settings: Maximum Delta Cn 0.05, a strict target FDR of 0.01, a relaxed target FDR of 0.05, and validation based on q-value. Protein identifications were accepted when the protein FDR was below 1% and when present in at least two out of three replicate injections with at least two peptides. The list of U937 mitochondrial proteins identified by MS/MS was generated by including the subset of mitochondrial protein sequences from UniprotKB Swiss-prot database, selected based on the “Mitochondrion” term of the “Cellular component” gene ontology (GO) category.

8.21 Bioinformatics Analysis

Functional enrichment based on GO categories was performed using FunRich open access software (<http://funrich.org/index.html>). The biological process enrichment network of identified mitochondrial proteins was constructed using the Network Analyst platform (<https://www.networkanalyst.ca>). A GOChord plot of selected GO categories extracted with the g:GOST tool of the g:Profiler toolset (<https://biit.cs.ut.ee/gprofiler/gost>) was drawn using the GOplot package v1.0.2 of the RStudio v1.2.1335 environment for R (<http://www.R-project.org>).

8.22 RNA purification

Cell pellets were briefly suspended in RNA Lysis Buffer (Quick-RNA Microprep Kit) and briefly shaken on vortex. 1 volume of ethanol (95-100%) (1: 1) was added to each sample and mixed well. The mixture was transferred to a Zymo-Spin IC column in a collection tube and centrifuged for 30 seconds eliminating the flow-through. This is followed by the additional DNase I Treatment in column step for the removal of trace DNA. The RNA Prep Buffer was added to the column and centrifuged for 30 seconds and discarded the flow-through. Two RNA washes and spin cycles were followed to complete the removal of the wash buffer. Then the column was carefully transferred to an RNase-free tube by adding 15 µl of DNase / RNase-free water and centrifuged for 30 seconds. Eluted RNA was quantized for subsequent experiments.

8.23 RT-PCR and quantitative real-time PCR analysis

Reverse transcription polymerase chain reaction (RT-PCR) was performed to measure the PGC1α mRNA levels in U937 cell line. The resulting cDNA was used for real time RT-PCR using SYBR Green Master Mix (Biorad). GAPDH primers were used as control.

8.24 KAPA RNA HyperPrep Kit with RiboErase (HMR)

600ng of total RNA input samples from U937 cells (control and treated) were used to assemble rRNA hybridization reaction followed by a depletion step containing RNase H before to proceed immediately to rRNA depletion cleanup. To remove the hybridization oligonucleotides from the ribosomal-depleted RNA, the samples were incubated with DNase at 37°C for 30 minutes. After the DNase digestion cleanup, the RNA depleted of rRNA is eluted from beads in Fragment, Prime and Elute Buffer (1x) and fragmented to the desired size by incubation at high temperature in the presence of Mg²⁺. On ice, the 1st strand synthesis reaction was assembled with random primers followed by the synthesis of 2nd strand cDNA which converts the cDNA:RNA hybrid into dscDNA, while marking the 2nd strand with dUTP. dAMP is then added to the 3' end of fragments of dscDNA. With the adapter ligation step, 3'-dTMP adapters are ligated to 3'-dAMP library fragments and immediately performed a 0.63X bead-based cleanup to lose unbound adapters. A 0.7X bead-based cleanup followed before to proceed with a library amplification step in which the adapter-ligated library DNA was amplified by PCR; dUTP marked strand was not amplified. The last 0.8X bead-based cleanup was performed, then the library fragment size distribution was confirmed by DeNovix Fluorometer. The RNA was ready for Illumina Platform.

8.25 RNA-seq analysis

RNAseq fastq files for U937 cell lines were aligned to the hg38 genome with STAR using the available manual. The GTF annotation file and DNA assembly fasta file were retrieved from ENSEMBL FTP43 and used to assemble the genome using `-runMode genomeGenerate`. The fastq files were aligned using the generated genome, with the paired-end experiments aligned together. The output BAM file was sorted by coordinate. The BAM files were converted to bigwig using `bamCoverage` with normalization to RPKM for visualization in the UCSC browser. Differentially expressed genes were identified by statistics analysis using edgeR package from bioconductor. The statistically significant threshold (FDR = 0.05) was applied. For visualization, fold changes larger than 1.5 and FDR of 0.01 were used to plot expression level of protein-coding genes.

REFERENCES

1. Carafa, V.; Nebbioso, A.; Cuomo, F.; Rotili, D.; Cobellis, G.; Bontempo, P.; Baldi, A.; Spugnini, E.P.; Citro, G.; Chambery, A.; et al. RIP1–HAT1–SIRT complex identification and targeting in treatment and prevention of cancer. *Clin Cancer Res.* **2018**, *24*, (12):2886–900. doi:10.1158/1078-0432.CCR-17-3081
2. Feinberg, A.P.; Ohlsson, R.; Henikoff, S. The epigenetic progenitor origin of human cancer. *Nat Rev Genet.* **2006**, *7*, (1):21–33. doi:10.1038/nrg1748
3. Miranda Furtado, C.L.; Dos Santos Luciano, M.C.; Silva Santos, R. Da.; Furtado, G.P.; Moraes, M.O.; Pessoa, C. Epidrugs: targeting epigenetic marks in cancer treatment. *Epigenetics.* **2019**, *14*, (12):1164–76. doi:10.1080/15592294.2019.1640546
4. Sharma, S.; Kelly, T.K.; Jones, P.A. Epigenetics in cancer. *Carcinogenesis.* **2009**, *31*, (1):27–36. doi:10.1093/carcin/bgp220
5. Dell’Aversana, C.; Lepore, I.; Altucci, L. HDAC modulation and cell death in the clinic. *Exp Cell Res.* **2012**, *318*, (11):1229–44. doi:10.1016/j.yexcr.2012.01.025
6. Galluzzi, L.; Bravo-San Pedro, J.M.; Vitale, I.; Aaronson, S.A.; Abrams, J.M.; Adam, D.; Alnemri, E.S.; Altucci, L.; Andrews, D.; Annicchiarico-Petruzzelli, M.; et al. Essential versus accessory aspects of cell death: Recommendations of the NCCD 2015. *Cell Death Differ.* **2015**, *22*, (1):58–73. doi:10.1038/cdd.2014.137
7. Galluzzi, L.; Vitale, I.; Aaronson, S.A.; Abrams, J.M.; Adam, D.; Agostinis, P.; Alnemri, E.S.; Altucci, L.; Amelio, I.; Andrews, D.W.; et al. Molecular mechanisms of cell death: Recommendations of the Nomenclature Committee on Cell Death 2018. *Cell Death Differ.* **2018**, *25*, (3):486–541. doi:10.1038/s41418-017-0012-4
8. Dhuriya, Y.K.; Sharma, D. Necroptosis: A regulated inflammatory mode of cell death. *J Neuroinflammation.* **2018**, *15*, (1):1–9. doi:10.1186/s12974-018-1235-0
9. Su, Z.; Yang, Z.; Xu, Y.; Chen, Y.; Yu, Q. Apoptosis, autophagy, necroptosis, and cancer metastasis. *Mol Cancer.* **2015**, *14*, (1):1–14. doi:10.1186/s12943-015-0321-5
10. Carafa, V.; Altucci, L. Deregulation of cell death in cancer: Recent highlights. *Cancers (Basel).* **2020**, *12*, (12):1–4. doi:10.3390/cancers12123517
11. Zhao, H.; Jaffer, T.; Eguchi, S.; Wang, Z.; Linkermann, A.; Ma, D. Role of necroptosis in the pathogenesis of solid organ injury. *Cell Death Dis.* **2015**, *6*, (11):1–10. doi:10.1038/cddis.2015.316

12. Molnár, T.; Mázló, A.; Tslaf, V.; Szöllósi, A.G.; Emri, G.; Koncz, G. Current translational potential and underlying molecular mechanisms of necroptosis. *Cell Death Dis.* **2019**, *10*, (11). doi:10.1038/s41419-019-2094-z
13. Ch'en, I.L.; Tsau, J.S.; Molkenstin, J.D.; Komatsu, M.; Hedrick, S.M. Mechanisms of necroptosis in T cells. *J Exp Med.* **2011**, *208*, (4):633–41. doi:10.1084/jem.20110251
14. Chen, D.; Yu, J.; Zhang, L. Necroptosis: an alternative cell death program defending against cancer. *Biochim Biophys Acta - Rev Cancer.* **2016**, *1865*, (2):228–36. doi:10.1016/j.bbcan.2016.03.003
15. Wang, T.; Jin, Y.; Yang, W.; Zhang, L.; Jin, X.; Liu, X.; He, Y.; Li, X. Necroptosis in cancer: An angel or a demon? *Tumor Biol.* **2017**, *39*, (6):101042831771153. doi:10.1177/1010428317711539
16. Su, Z.; Yang, Z.; Xie, L.; Dewitt, J.P.; Chen, Y. Cancer therapy in the necroptosis era. *Cell Death Differ.* **2016**, *23*, (5):748–56. doi:10.1038/cdd.2016.8
17. Galluzzi, L.; Vitale, I.; Abrams, J.M.; Alnemri, E.S.; Baehrecke, E.H.; Blagosklonny, M. V.; Dawson, T.M.; Dawson, V.L.; El-Deiry, W.S.; Fulda, S.; et al. Molecular definitions of cell death subroutines: recommendations of the Nomenclature Committee on Cell Death 2012. *Cell Death Differ.* **2012**, *19*, (1):107–20. doi:10.1038/cdd.2011.96
18. Dunai, Z.; Bauer, P.I.; Mihalik, R. Necroptosis: Biochemical, physiological and pathological aspects. *Pathol Oncol Res.* **2011**, *17*, (4):791–800. doi:10.1007/s12253-011-9433-4
19. Su, Z.; Yang, Z.; Xie, L.; Dewitt, J.P.; Chen, Y. Cancer therapy in the necroptosis era. **2016**, :748–56. doi:10.1038/cdd.2016.8
20. Gong, Y.; Fan, Z.; Luo, G.; Yang, C.; Huang, Q.; Fan, K.; Cheng, H.; Jin, K.; Ni, Q.; Yu, X.; et al. The role of necroptosis in cancer biology and therapy. *Mol Cancer.* **2019**, *18*, (1):1–17. doi:10.1186/s12943-019-1029-8
21. Zhang, D.; Lin, J.; Han, J. Receptor-interacting protein (RIP) kinase family. *Cell Mol Immunol.* **2010**, *7*, (4):243–9. doi:10.1038/cmi.2010.10
22. Moriwaki, K.; Bertin, J.; Gough, P.J.; Orłowski, G.M.; Chan, F.K.M. Differential roles of RIPK1 and RIPK3 in TNF-induced necroptosis and chemotherapeutic agent-induced cell death. *Cell Death Dis.* **2015**, *6*, (2):e1636-11. doi:10.1038/cddis.2015.16
23. Fagerberg, L.; Hallstrom, B.M.; Oksvold, P.; Kampf, C.; Djureinovic, D.; Odeberg, J.; Habuka, M.; Tahmasebpour, S.; Danielsson, A.; Edlund, K.; et al. Analysis of the human tissue-specific expression by genome-wide integration of transcriptomics and antibody-based proteomics. *Mol Cell Proteomics.* **2014**, *13*, (2):397–406. doi:10.1074/mcp.M113.035600

24. Buchrieser, J.; Oliva-Martin, M.J.; Moore, M.D.; Long, J.C.D.; Cowley, S.A.; Perez-Simón, J.A.; James, W.; Venero, J.L. RIPK1 is a critical modulator of both tonic and TLR-responsive inflammatory and cell death pathways in human macrophage differentiation. *Cell Death Dis.* **2018**, *9*, (10):973. doi:10.1038/s41419-018-1053-4
25. Lafont, E.; Draber, P.; Rieser, E.; Reichert, M.; Kupka, S.; de Miguel, D.; Draberova, H.; von Mässenhausen, A.; Bhamra, A.; Henderson, S.; et al. TBK1 and IKK ϵ prevent TNF-induced cell death by RIPK1 phosphorylation. *Nat Cell Biol.* **2018**, *20*, (12):1389–99. doi:10.1038/s41556-018-0229-6
26. Xu, D.; Jin, T.; Zhu, H.; Chen, H.; Ofengeim, D.; Zou, C.; Mifflin, L.; Pan, L.; Amin, P.; Li, W.; et al. TBK1 Suppresses RIPK1-Driven Apoptosis and Inflammation during Development and in Aging. *Cell.* **2018**, *174*, (6):1477-1491.e19. doi:10.1016/j.cell.2018.07.041
27. Shan, B.; Pan, H.; Najafov, A.; Yuan, J. Necroptosis in development and diseases. *Genes Dev.* **2018**, *32*, (5–6):327–40. doi:10.1101/gad.312561.118
28. Dondelinger, Y.; Delanghe, T.; Priem, D.; Wynosky-Dolfi, M.A.; Sorobetea, D.; Rojas-Rivera, D.; Giansanti, P.; Roelandt, R.; Gropengiesser, J.; Ruckdeschel, K.; et al. Serine 25 phosphorylation inhibits RIPK1 kinase-dependent cell death in models of infection and inflammation. *Nat Commun.* **2019**, *10*, (1):1729. doi:10.1038/s41467-019-09690-0
29. Tait, S.W.G.; Ichim, G.; Green, D.R. Die another way – non-apoptotic mechanisms of cell death. *J Cell Sci.* **2014**, *127*, (10):2135–44. doi:10.1242/jcs.093575
30. Zhu, F.; Zhang, W.; Yang, T.; He, S. dan. Complex roles of necroptosis in cancer. *J Zhejiang Univ Sci B.* **2019**, *20*, (5):399–413. doi:10.1631/jzus.B1900160
31. Najafov, A.; Chen, H.; Yuan, J. Necroptosis and Cancer. *Trends in Cancer.* **2017**, *3*, (4):294–301. doi:10.1016/j.trecan.2017.03.002
32. Wegner, K.W.; Saleh, D.; Degterev, A. Complex Pathologic Roles of RIPK1 and RIPK3: Moving Beyond Necroptosis. *Trends Pharmacol Sci.* **2017**, *38*, (3):202–25. doi:10.1016/j.tips.2016.12.005
33. Rickard, J.A.; O'Donnell, J.A.; Evans, J.M.; Lalaoui, N.; Poh, A.R.; Rogers, T.; Vince, J.E.; Lawlor, K.E.; Ninnis, R.L.; Anderton, H.; et al. RIPK1 regulates RIPK3-MLKL-driven systemic inflammation and emergency hematopoiesis. *Cell.* **2014**, *157*, (5):1175–88. doi:10.1016/j.cell.2014.04.019
34. Wang, Q.; Fan, D.; Xia, Y.; Ye, Q.; Xi, X.; Zhang, G.; Xiao, C. The latest information on the RIPK1 post-translational modifications and functions. *Biomed Pharmacother.* **2021**, *142*, (April):112082. doi:10.1016/j.biopha.2021.112082
35. Dondelinger, Y.; Darding, M.; Bertrand, M.J.M.; Walczak, H. Poly-ubiquitination in TNFR1-mediated

necroptosis. *Cell Mol Life Sci.* **2016**, *73*, (11–12):2165–76. doi:10.1007/s00018-016-2191-4

36. Della Torre, L.; Nebbioso, A.; Stunnenberg, H.G.; Martens, J.H.A.; Carafa, V.; Altucci, L. The Role of Necroptosis: Biological Relevance and Its Involvement in Cancer. *Cancers (Basel)*. **2021**, *13*, (4):684. doi:10.3390/cancers13040684
37. Ermine, K.; Yu, J.; Zhang, L. Role of Receptor Interacting Protein (RIP) kinases in cancer. *Genes Dis.* **2021**, (xxxx). doi:10.1016/j.gendis.2021.10.007
38. Tate, J.G.; Bamford, S.; Jubb, H.C.; Sondka, Z.; Beare, D.M.; Bindal, N.; Boutselakis, H.; Cole, C.G.; Creatore, C.; Dawson, E.; et al. COSMIC: The Catalogue Of Somatic Mutations In Cancer. *Nucleic Acids Res.* **2019**, *47*, (D1):D941–7. doi:10.1093/nar/gky1015
39. McCormick, K.D.; Ghosh, A.; Trivedi, S.; Wang, L.; Coyne, C.B.; Ferris, R.L.; Sarkar, S.N. Innate immune signaling through differential RIPK1 expression promote tumor progression in head and neck squamous cell carcinoma. *Carcinogenesis*. **2016**, *37*, (5):522–9. doi:10.1093/carcin/bgw032
40. Schwabe, R.F.; Luedde, T. Apoptosis and necroptosis in the liver: a matter of life and death. *Nat Rev Gastroenterol Hepatol.* **2018**, *15*, (12):738–52. doi:10.1038/s41575-018-0065-y
41. Yin, Z.; Chen, W.; Yin, J.; Sun, J.; Xie, Q.; Wu, M.; Zeng, F.; Ren, H. RIPK1 is a negative mediator in Aquaporin 1-driven triple-negative breast carcinoma progression and metastasis. *npj Breast Cancer*. **2021**, *7*, (1):1–11. doi:10.1038/s41523-021-00261-5
42. Park, S.; Hatanpaa, K.J.; Xie, Y.; Mickey, B.E.; Madden, C.J.; Raisanen, J.M.; Ramnarain, D.B.; Xiao, G.; Saha, D.; Boothman, D.A.; et al. The receptor interacting protein 1 inhibits p53 induction through NF- κ B activation and confers a worse prognosis in glioblastoma. *Cancer Res.* **2009**, *69*, (7):2809–16. doi:10.1158/0008-5472.CAN-08-4079
43. Wang, Q.; Chen, W.; Xu, X.; Li, B.; He, W.; Padilla, M.T.; Jang, J.H.; Nyunoya, T.; Amin, S.; Wang, X.; et al. RIP1 potentiates BPDE-induced transformation in human bronchial epithelial cells through catalase-mediated suppression of excessive reactive oxygen species. *Carcinogenesis*. **2013**, *34*, (9):2119–28. doi:10.1093/carcin/bgt143
44. Seifert, L.; Werba, G.; Tiwari, S.; Giao Ly, N.N.; Alothman, S.; Alqunaibit, D.; Avanzi, A.; Barilla, R.; Daley, D.; Greco, S.H.; et al. The necrosome promotes pancreatic oncogenesis via CXCL1 and Mincle-induced immune suppression. *Nature*. **2016**, *532*, (7598):245–9. doi:10.1038/nature17403
45. Zhu, G.; Ye, J.; Huang, Y.; Zheng, W.; Hua, J.; Yang, S.; Zhuang, J.; Wang, J. Receptor-interacting protein-1 promotes the growth and invasion in gastric cancer. *Int J Oncol.* **2016**, *48*, (6):2387–98. doi:10.3892/ijo.2016.3455

46. Liu, X.Y.; Lai, F.; Yan, X.G.; Jiang, C.C.; Guo, S.T.; Wang, C.Y.; Croft, A.; Tseng, H.-Y.; Wilmott, J.S.; Scolyer, R.A.; et al. RIP1 Kinase Is an Oncogenic Driver in Melanoma. *Cancer Res.* **2015**, *75*, (8):1736–48. doi:10.1158/0008-5472.CAN-14-2199
47. Zhu, G.; Chen, X.; Wang, X.; Li, X.; Du, Q.; Hong, H.; Tang, N.; She, F.; Chen, Y. Expression of the RIP-1 gene and its role in growth and invasion of human gallbladder carcinoma. *Cell Physiol Biochem.* **2014**, *34*, (4):1152–62. doi:10.1159/000366328
48. Lake, S.L.; Damato, B.E.; Kalirai, H.; Dodson, A.R.; Taktak, A.F.G.; Lloyd, B.H.; Coupland, S.E. Single nucleotide polymorphism array analysis of uveal melanomas reveals that amplification of CNKSR3 is correlated with improved patient survival. *Am J Pathol.* **2013**, *182*, (3):678–87. doi:10.1016/j.ajpath.2012.11.036
49. Zheng, X. lian.; Yang, J. jiao.; Wang, Y. yun.; Li, Q.; Song, Y. ping.; Su, M.; Li, J. ke.; Zhang, L.; Li, Z. ping.; Zhou, B.; et al. RIP1 promotes proliferation through G2/M checkpoint progression and mediates cisplatin-induced apoptosis and necroptosis in human ovarian cancer cells. *Acta Pharmacol Sin.* **2020**, *41*, (9):1223–33. doi:10.1038/s41401-019-0340-7
50. Gao, Q.; Liang, W.-W.; Foltz, S.M.; Mutharasu, G.; Jayasinghe, R.G.; Cao, S.; Liao, W.-W.; Reynolds, S.M.; Wyczalkowski, M.A.; Yao, L.; et al. Driver Fusions and Their Implications in the Development and Treatment of Human Cancers. *Cell Rep.* **2018**, *23*, (1):227-238.e3. doi:10.1016/j.celrep.2018.03.050
51. Yoshihara, K.; Wang, Q.; Torres-Garcia, W.; Zheng, S.; Vegesna, R.; Kim, H.; Verhaak, R.G.W. The landscape and therapeutic relevance of cancer-associated transcript fusions. *Oncogene.* **2015**, *34*, (37):4845–54. doi:10.1038/onc.2014.406
52. Hu, X.; Wang, Q.; Tang, M.; Barthel, F.; Amin, S.; Yoshihara, K.; Lang, F.M.; Martinez-Ledesma, E.; Lee, S.H.; Zheng, S.; et al. TumorFusions: an integrative resource for cancer-associated transcript fusions. *Nucleic Acids Res.* **2018**, *46*, (D1):D1144–9. doi:10.1093/nar/gkx1018
53. Shah, N.; Lankerovich, M.; Lee, H.; Yoon, J.-G.; Schroeder, B.; Foltz, G. Exploration of the gene fusion landscape of glioblastoma using transcriptome sequencing and copy number data. *BMC Genomics.* **2013**, *14*, (1):818. doi:10.1186/1471-2164-14-818
54. Hillert, L.K.; Bettermann-Bethge, K.; Nimmagadda, S.C.; Fischer, T.; Naumann, M.; Lavrik, I.N. Targeting RIPK1 in AML cells carrying FLT3-ITD. *Int J cancer.* **2019**, *145*, (6):1558–69. doi:10.1002/ijc.32246
55. Xin, J.; You, D.; Breslin, P.; Li, J.; Zhang, J.; Wei, W.; Cannova, J.; Volk, A.; Gutierrez, R.; Xiao, Y.; et al. Sensitizing acute myeloid leukemia cells to induced differentiation by inhibiting the RIP1 / RIP3

pathway. **2017**, (October 2016):1154–65. doi:10.1038/leu.2016.287

56. Seong, D.; Jeong, M.; Seo, J.; Lee, J.Y.; Hwang, C.H.; Shin, H.C.; Shin, J.Y.; Nam, Y.W.; Jo, J.Y.; Lee, H.; et al. Identification of MYC as an antineoplastic protein that stifles RIPK1–RIPK3 complex formation. *Proc Natl Acad Sci U S A*. **2020**, *117*, (33):19982–93. doi:10.1073/PNAS.2000979117
57. Obba, S.; Hizir, Z.; Boyer, L.; Selimoglu-Buet, D.; Pfeifer, A.; Michel, G.; Hamouda, M.A.; Gonçalves, D.; Cerezo, M.; Marchetti, S.; et al. The PRKAA1/AMPK α 1 pathway triggers autophagy during CSF1-induced human monocyte differentiation and is a potential target in CMML. *Autophagy*. **2015**, *11*, (7):1114–29. doi:10.1080/15548627.2015.1034406
58. Montalban-Bravo, G.; Class, C.A.; Ganan-Gomez, I.; Kanagal-Shamanna, R.; Sasaki, K.; Richard-Carpentier, G.; Naqvi, K.; Wei, Y.; Yang, H.; Soltysiak, K.A.; et al. Transcriptomic analysis implicates necroptosis in disease progression and prognosis in myelodysplastic syndromes. *Leukemia*. **2020**, *34*, (3):872–81. doi:10.1038/s41375-019-0623-5
59. Nugues, A.-L.; El Bouazzati, H.; Héтуin, D.; Berthon, C.; Loyens, A.; Bertrand, E.; Jouy, N.; Idziorek, T.; Quesnel, B. RIP3 is downregulated in human myeloid leukemia cells and modulates apoptosis and caspase-mediated p65/RelA cleavage. *Cell Death Dis*. **2014**, *5*, (8):e1384–e1384. doi:10.1038/cddis.2014.347
60. Bruzzoni-Giovanelli, H.; González, J.R.; Sigaux, F.; Villoutreix, B.O.; Cayuela, J.M.; Guilhot, J.; Preudhomme, C.; Guilhot, F.; Poyet, J.-L.; Rousselot, P. Genetic polymorphisms associated with increased risk of developing chronic myelogenous leukemia. *Oncotarget*. **2015**, *6*, (34):36269–77. doi:10.18632/oncotarget.5915
61. Park, C.; Han, S.; Lee, K.-M.; Choi, J.-Y.; Song, N.; Jeon, S.; Park, S.K.; Ahn, H.S.; Shin, H.Y.; Kang, H.J.; et al. Association between CASP7 and CASP14 genetic polymorphisms and the risk of childhood leukemia. *Hum Immunol*. **2012**, *73*, (7):736–9. doi:10.1016/j.humimm.2012.04.017
62. Xu, X.; Kalac, M.; Markson, M.; Chan, M.; Brody, J.D.; Bhagat, G.; Ang, R.L.; Legarda, D.; Justus, S.J.; Liu, F.; et al. Reversal of CYLD phosphorylation as a novel therapeutic approach for adult T-cell leukemia/lymphoma (ATLL). *Cell Death Dis*. **2020**, *11*, (2):94. doi:10.1038/s41419-020-2294-6
63. Löder, S.; Fakler, M.; Schoeneberger, H.; Cristofanon, S.; Leibacher, J.; Vanlangenakker, N.; Bertrand, M.J.M.; Vandenabeele, P.; Jeremias, I.; Debatin, K.-M.; et al. RIP1 is required for IAP inhibitor-mediated sensitization of childhood acute leukemia cells to chemotherapy-induced apoptosis. *Leukemia*. **2012**, *26*, (5):1020–9. doi:10.1038/leu.2011.353
64. Huang, X.; Xiao, F.; Li, Y.; Qian, W.; Ding, W.; Ye, X. Bypassing drug resistance by triggering

necroptosis: Recent advances in mechanisms and its therapeutic exploitation in leukemia. *J Exp Clin Cancer Res.* **2018**, *37*, (1):1–15. doi:10.1186/s13046-018-0976-z

65. Martens, S.; Hofmans, S.; Declercq, W.; Augustyns, K.; Vandenabeele, P. Inhibitors Targeting RIPK1/RIPK3: Old and New Drugs. *Trends Pharmacol Sci.* **2020**, *41*, (3):209–24. doi:10.1016/j.tips.2020.01.002
66. Hou, J.; Ju, J.; Zhang, Z.; Zhao, C.; Li, Z.; Zheng, J.; Sheng, T.; Zhang, H.; Hu, L.; Yu, X.; et al. Discovery of potent necroptosis inhibitors targeting RIPK1 kinase activity for the treatment of inflammatory disorder and cancer metastasis. *Cell Death Dis.* **2019**, *10*, (7). doi:10.1038/s41419-019-1735-6
67. Mifflin, L.; Ofengeim, D.; Yuan, J. Receptor-interacting protein kinase 1 (RIPK1) as a therapeutic target. *Nat Rev Drug Discov.* **2020**, *19*, (8):553–71. doi:10.1038/s41573-020-0071-y
68. Carafa, V.; Poziello, A.; Torre, L.D.; Giovannelli, P.; Di Donato, M.; Safadeh, E.; Yu, Z.; Baldi, A.; Castoria, G.; Tomaselli, D.; et al. Enzymatic and biological characterization of novel sirtuin modulators against cancer. *Int J Mol Sci.* **2019**, *20*, (22). doi:10.3390/ijms20225654
69. Porporato, P.E.; Filigheddu, N.; Pedro, J.M.B.-S.; Kroemer, G.; Galluzzi, L. Mitochondrial metabolism and cancer. *Cell Res.* **2018**, *28*, (3):265–80. doi:10.1038/cr.2017.155
70. Zhang, Y.; Su, S.S.; Zhao, S.; Yang, Z.; Zhong, C.Q.; Chen, X.; Cai, Q.; Yang, Z.H.; Huang, D.; Wu, R.; et al. RIP1 autophosphorylation is promoted by mitochondrial ROS and is essential for RIP3 recruitment into necrosome. *Nat Commun.* **2017**, *8*, (May 2016):1–14. doi:10.1038/ncomms14329
71. Badrinath, N.; Yoo, S.Y. Mitochondria in cancer: in the aspects of tumorigenesis and targeted therapy. *Carcinogenesis.* **2018**, *39*, (12):1419–30. doi:10.1093/carcin/bgy148
72. Austin, S.; St-Pierre, J. PGC1 α and mitochondrial metabolism – emerging concepts and relevance in ageing and neurodegenerative disorders. *J Cell Sci.* **2012**, *125*, (21):4963–71. doi:10.1242/jcs.113662
73. Hanahan, D.; Weinberg, R.A. Hallmarks of cancer: The next generation. *Cell.* **2011**, *144*, (5):646–74. doi:10.1016/j.cell.2011.02.013
74. Stack, H.; Hill, C.; Gahan, C. Stress Responses. In: Handbook of Listeria Monocytogenes. CRC Press; 2008. p. 61–96. doi:10.1201/9781420051414.ch3